Pressure-Transient Analysis of Bottomhole Pressure and Rate Measurements by Use of System-Identification Techniques

M. Mansoori, Delft University of Technology and Sharif University of Technology;
P. M. J. Van den Hof, Eindhoven University of Technology; **J.-D. Jansen,** Delft University of Technology;
and **D. Rashtchian,** Sharif University of Technology

Summary

This study presents a novel perspective on pressure-transient analysis (PTA) of downhole-pressure and flow-rate data by use of system-identification (SI) techniques as widely used in advanced process engineering. Key features of the paper are that it considers the classic PTA process from a system-theoretical perspective; derives the causal structure of the flow dynamics; proposes a method to deal with continuously varying pressure and flow-rate signals contaminated with correlated noise, which estimates physical reservoir parameters through a systematic matching procedure in the frequency domain; and can cope with arbitrary (i.e., not necessarily piecewise constant) flow-rate signals. To this end, the wellbore and the reservoir are modeled as two distinct two-port power-transmitting systems that are bilaterally coupled at their common boundary. This structure reveals that, from an SI perspective, the wellbore dynamics affect the bottomhole data as a feedback mechanism. Because of this feedback structure, it is necessary to use closed-loop SI techniques, and, because of the presence of sensor noise, the reservoir model cannot be identified solely from the bottomhole measurements. Therefore, an auxiliary signal is needed, for which we choose the surface flow rate, although other signals, such as the bottomhole temperature, could potentially also be used. Then a suitable closed-loop SI technique is the so-called two-stage method. The first stage of the algorithm removes the dynamic effects of the wellbore from the noisy data, and the second stage identifies the reservoir model in terms of rational polynomials. Thereafter, the usual physical reservoir parameters (e.g., averaged permeability and skin factor) are obtained through matching the results of the identified reservoir model and those of typical analytical reservoir models in the frequency domain, as an alternative to classic graphical or numerical type-curve analysis. The method does not rely on a piecewise constant approximation of the flow-rate signal, unlike other known PTA methods such as time-domain deconvolution. Six numerical experiments, by use of a synthetic data set, and one field example, by use of data from a real gas well, illustrate the key aspects of the proposed method.

Introduction

Traditional pressure-transient analysis (PTA), also called buildup testing or well testing, relies on the use of downhole-pressure measurements (from retrievable or permanent gauges) in combination with a fixed flow rate, where the most-reliable form of a fixed rate is a zero rate obtained by a quick-closing downhole valve during drillstem testing. More-inaccurate "zero" rates are obtained by shutting in the well at surface and accounting for the wellbore-storage effect (resulting in an initial nonzero rate at the bottom of the well) with the aid of a simple model (a wellbore-storage coefficient). In conventional PTA, the step response in the bottomhole pressure resulting from shutting in the well is used to identify the reservoir type through type-curve matching—through comparison of the shape of the measured response to those of known "typical" reservoir types selected on the basis of prior information such as well type, completion details, or log data—and to estimate physical reservoir parameters (e.g., average permeability and skin factor) by identifying characteristic slopes or by manual or computer-aided adjustment of the parameters of the response model for the selected reservoir type until the corresponding pressure response matches the measured response. An obvious disadvantage of conventional PTA is the need to shut in the well, leading to deferred production.

The widespread availability of permanent downhole-pressure gauges, in combination with the emerging use of permanent downhole sensors for (total) flow rate, has inspired a new area of research in the field of PTA over the past decade. The availability of permanent downhole-pressure and rate measurements potentially allows for frequent PTA without the need to shut in the well, by use of fluctuations in bottomhole pressure and flow rate resulting from operational disturbances, such as closing in a neighboring well, or deliberate changes in operating conditions. In the literature, several methods have been proposed to modify the first step of PTA (reservoir-type identification) to cope with nonconstant-flow rates. Generally, it is assumed that the governing partial-differential equation for single-phase flow in a reservoir is approximately linear. Hence, Duhamel's principle is valid, and consequently the bottomhole-pressure change with respect to the initial reservoir pressure is described as the convolution of the flow rate into the well with the impulse (pressure) response of the reservoir. The problem to be solved in this step is therefore to compute the impulse response of the reservoir from the bottomhole pressure and flow-rate measurements, a process known as deconvolution in the PTA literature (Kuchuk et al. 2010). Once the impulse response is known, it is possible to generate the corresponding step response and proceed with the conventional PTA procedure as if the step response had been obtained by shutting in the well. The deconvolution problem has been addressed by several researchers (Roumboutsos and Stewart 1988; Bourgeois and Horne 1993; Baygü et al. 1997; Onur and Reynolds 1998; Gringarten 2008). For a recent review we refer to Kamal and Abbaszadeh (2009) and Kuchuk et al. (2010).

The main challenge in the use of deconvolution methods for well-test analysis is their high level of sensitivity to the presence of noise. The algorithms typically become unstable in cases with even a relatively low sensor-noise level in one of the measured variables. Realistically, both bottomhole-pressure and flow-rate measurements contain sensor noise, and without properly dealing with the noise, the estimate of the reservoir's impulse response will be biased and maybe even uninterpretable. Note that in addition to sensor noise, the effects of disturbances such as turbulence in the wellbore are present in the measurements. Von Schroeter et al. (2004) and Levitan (2005) propose two similar robust and stable algorithms that can handle relatively high levels of sensor noise in both measured variables by modeling the noise as uncorrelated Gaussian signals. These algorithms solve a nonlinear, regularized total-least-square (TLS) -optimization problem to estimate the reservoir's impulse response. However to implement the algorithm, certain regularization parameters need to be selected a

Copyright © 2015 Society of Petroleum Engineers

Original SPE manuscript received for review 18 July 2014. Revised manuscript received for review 4 June 2015. Paper (SPE 176031) peer approved 9 June 2015.

priori. Unfortunately, the final estimate is very sensitive to the chosen values of the regularization parameters, the optimal values of which depend on the properties of the noise (such as variance) and on penalty terms associated with the curvature of the response that are very difficult to know, if at all, a priori. Pimonov et al. (2010) modified the TLS method of von Schroeter et al. (2004) by introducing a weighting factor to emphasize those measurements that are assumed to have low sensor noise, thus increasing the number of tuning variables.

An important limiting factor of all TLS-based algorithms is that they require a piecewise-constant approximation of the flow-rate signal. We note that this is not a theoretical limitation but rather the effect of a numerical implementation in which the flow rate is discretized in a piecewise-constant fashion. To approximate the signal as a series of constant-rate-flow periods, the exact starting points of the periods are usually found on the basis of breakpoints in the measured pressure signal (Athichanagorn 1999). Unfortunately, sensor noise often masks the exact location of the breakpoints, and, consequently, breakpoint-detection algorithms may not always find the exact starting points of the flow periods. Especially for measurements with many short flow periods, these errors can affect the estimated response considerably (Nomura and Horne 2009).

Cheng et al. (2005) consider the analysis of data sets with completely variable flow rates by use of a deconvolution algorithm modeled after a frequency-domain transformation of the measurements. In the frequency domain, the convolution integral becomes a simple algebraic equation and the quotient of the Fourier transform of the pressure and flow-rate signals gives the Fourier transform of the impulse-response function. The impulse response of the reservoir is then calculated by inverse-Fourier transformation of the solution. Because the frequency transformation does not need any assumption on the shape of the flow-rate signal in the time domain, the algorithm can be applied to data sets with continuously varying flow-rate signals. However, the simple algebraic equation is no longer valid when the data contain noise, and therefore the authors propose an iterative scheme to suppress the noise in the data and calculate the impulse response. Although the algorithm appears simple to deploy, the study does not provide any statistical or mathematical analysis to assess its accuracy.

Next, we consider the two main steps of PTA: reservoir-type characterization and physical-parameter estimation. We assume that the identified reservoir model has been obtained in the form of a bottomhole-pressure-step response, either through direct measurement of the pressure in response to shutting in the well or through deconvolution of continuous pressure and flow-rate signals. A graphical representation of the identified model—typically a log-log plot of the Bourdet derivative (i.e., the pressure derivative with respect to the natural logarithm of time vs. time)—is then compared with graphical-model representations of known "typical"-reservoir models (referred to as type curves) selected on the basis of prior information such as well type, completion details, and log data. The reservoir-flow regime and the presence of flow-relevant heterogeneities are determined through selection of the type curve that best fits the features (slopes, curvatures, and asymptotes) of the identified model. The "typical"-reservoir models are obtained as (semi-) analytical solutions of the governing differential equations for single-phase flow in relatively simple geometries, with parameters that represent physical parameters such as average permeability, skin factor, and drainage radius. These parameters are then estimated by minimizing some difference measure between the graphical representations of the identified and the selected known reservoir models. The (semi-) analytical solutions are usually obtained in the Laplace domain. However, the parameter estimation is usually dependent on comparisons in the time domain, which, therefore, requires taking the inverse Laplace transform of the analytical solution. To avoid this transformation, Bourgeois and Horne (1993) proposed to perform the physical-parameter estimation in the Laplace domain, whereas more recently, Ahn and Horne (2011) introduced an estimation method in the frequency domain.

This paper studies the PTA problem from a system-theoretical perspective, and presents a new method to analyze continuously varying pressure and rate data. It proposes the use of system-identification (SI) techniques to identify a data-driven reservoir model. SI is the process of identifying a mathematical model with rigorous error estimates, on the basis of measured input and output data, and has been widely used in control engineering and advanced process engineering (Ljung 1999). To our knowledge, the use of SI methods on the well-testing problem has not been attempted before, except for work reported by Kuiper (2009). To apply SI, the causal structure (input/output relationship) of the system needs to be known. Consequently, to use SI for well-test analysis, first the causal structure of production system must be determined. For this, we consider the reservoir and wellbore as two distinct systems that interact at the bottom of the hole. The wellbore and reservoir can each be modeled as two-port hydraulic-power-transfer (sub)systems, where the power flow (i.e., the time derivative of energy) at a certain point in the system is equal to the product of flow rate and pressure at that point. The interaction between the two subsystems is modeled by bilaterally coupling them (i.e., by requiring equality of both pressure and flow rate at the interface). As will be illustrated in detail in this study, the resultant structure reveals that the wellbore dynamics act as a feedback between the bottomhole pressure and flow rate.

Because of the feedback structure of the coupled well/reservoir system, it is necessary to use closed-loop SI techniques. We will show that, in the presence of noise, the reservoir model cannot be identified solely from the bottomhole measurements, and that an auxiliary signal is needed to make the identification feasible. In this paper, we choose the surface flow rate as the auxiliary signal. Then, a suitable closed-loop SI technique is used: the so-called two-stage (TS) method (Van den Hof and Schrama 1993). In the first stage, a noise-free bottomhole-flow-rate signal is estimated. In the second stage, this signal is used to identify the reservoir model without wellbore effects. Subsequently, the identified reservoir model is transformed to the frequency domain, and the reservoir type is characterized. The physical parameters are then estimated on the basis of a comparison of the identified model with a physics-based model in the frequency domain. The particular TS SI method presented in this study relies on the availability of an external-control signal and on the presence of near-linear dynamic relationships between flow rate and pressure in both the wellbore and the reservoir. If these conditions are satisfied, then measurements with completely variable flow rate and correlated sensor noise, and that are contaminated by the effects of unknown disturbances such as turbulence, can be handled effectively. In the synthetic examples treated in this study, we have chosen the external-control signal in the form of a nearly noise-free surface flow-rate measurement, and in the (single-phase) field example in the form of set-point surface flow rates. It is, in theory, also possible to use (single-phase) surface choke settings (which are nonlinearly related to the flow rate) by use of the modified TS method presented in Forssell and Ljung (1999). For single-phase wellbore flow (e.g., in water-injection wells or dead-oil- or dry-gas-production wells) it is indeed possible to obtain nearly noise-free surface flow-rate measurements. For multiphase (live-oil- or wet-gas-production wells), this is not feasible. Although the requirement of noise-free surface rate measurements is therefore restrictive, we note that most parts of our theoretical development will remain valid for more-general SI methods, including those relying on different auxiliary signals, either with or without noise. Depending on the nature of such an alternative auxiliary signal, specific SI methods may be required, the description of which is outside the scope of this paper. First steps toward such a more-generally-applicable SI method have been reported in Mansoori et al. (2014), where we used surface flow-rate measurements contaminated with sensor noise, and in Mansoori et al. (*in press*), where bottomhole-temperature measurements are used as the auxiliary variable.

The study is organized as follows. In the second section, Modeling the Production System, the modeling of the wellbore and the reservoir and the coupling between the models are explained in

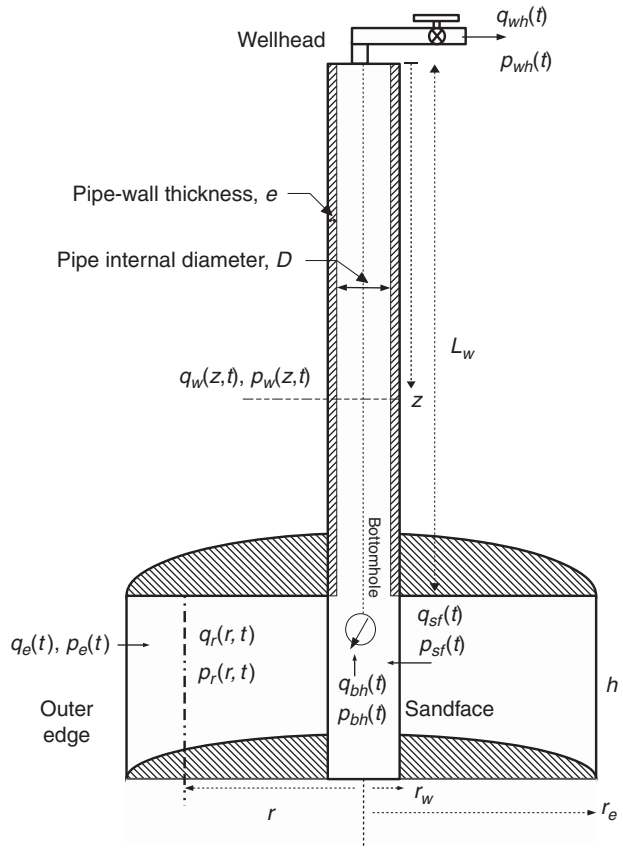

Fig. 1—A cylindrical homogeneous reservoir with a vertical well where the wellhead flow rate is controlled, and the bottomhole flow rate and pressure are measured.

detail. In the third section, Model Identification and Parameter Estimation, SI is concisely explained and the application of TS closed-loop SI to well-test data is elaborated on. (A more-elaborate description of the basics of SI is given in Appendix A.) Physical-parameter estimation in the frequency domain is explained in the fourth section, Physical-Parameter Estimation. The results of model identification and parameter estimation for synthetic examples and a field case are discussed in the sections Synthetic Examples and Field Example, respectively, and the final section is Conclusions.

Modeling the Production System

Introduction. System identification, just like the parameter-estimation step in classical well testing, involves matching the output of a system model to the measured output, and just like in classical well testing we need prior information to determine the nature of the reservoir model. In this section, we present a system model in the form of a simple cylindrical and homogeneous reservoir drained by a vertical well in its center **(Fig. 1).** This model also allows us to analyze the well-test process from a system-theoretical perspective and derive its corresponding causal structure. We assume that the well test is carried out by manipulating the choke at the wellhead and measuring the resulting bottomhole-flow rate and pressure. The reservoir and the wellbore are modeled as two distinct fluid-delivery systems, coupled at the bottom of the well. To derive the dynamical relationships of the wellbore and reservoir analytically, we assume, as a first step, that the reservoir and the wellbore contain a slightly compressible single-phase fluid. During a well test the wellbore will usually experience two-phase flow in at least the top part of the well. Modeling the dynamical behavior of this two-phase flow in detail is out of the scope of this study. However, in a second step, we will follow the usual approach in conventional pressure-transient analysis (PTA) to approximate the wellbore dynamics with a single wellbore-storage (WBS) coefficient.

Modeling the Fluid Flow in the Wellbore. ***Single-Phase-Liquid-Flow Model.*** The fluid enters the production tubing at the bottom of the well with flow rate $q_{bh}(t)$ and bottomhole pressure $p_{bh}(t)$. The fluid reaches the top of the well with flow rate $q_{wh}(t)$ and wellhead pressure $p_{wh}(t)$. Let $q_w(z,t)$ and $p_w(z,t)$ be the flow rate and pressure in the tubing at depth z and time t, respectively. [Note that throughout this study we assume that all flow rates and pressures $q_x(t)$ and $p_x(t)$, with x representing an arbitrary subscript, are flow rate and pressure differences with respect to the steady-state condition. The constant hydrostatic pressure in the well is therefore not part of $p(t)$.] In general, the dynamics of unsteady flow within the tubing can be modeled with the aid of mass-, momentum-, and energy-conservation equations. As a first step, we consider isothermal flow of a single-phase, constant-density, slightly compressible liquid through an elastic pipe of constant cross section, which are relevant assumptions for water-injection wells. (If necessary, the equations can simply be extended to a quasi-isothermal situation with temperature-dependent fluid properties and a temperature profile along the well that is defined a priori.) In this case, these equations are reduced to two water-hammer equations (Chaudhry 1979), which describe the relationships between $q_w(z,t)$ and $p_w(z,t)$ as

$$\frac{\rho a^2}{A}\frac{\partial q_w(z,t)}{\partial z}+\frac{\partial p_w(z,t)}{\partial t}=0, \quad \ldots\ldots\ldots\ldots\ldots\ldots (1)$$

$$\frac{A}{\rho}\frac{\partial p_w(z,t)}{\partial z}+\frac{\partial q_w(z,t)}{\partial t}+Rq_w(z,t)=0, \quad \ldots\ldots\ldots\ldots (2)$$

where g is acceleration of gravity (9.81 m/s^2), A is cross-sectional area of the pipe (m^2), ρ is fluid density (kg/m^3), $a^2=K/[\rho+KD\rho(eE)^{-1}]$ is velocity of water-hammer wave in the fluid (m/s), $R=32\ \nu/D^2$ is laminar-flow-friction effect (1/s), K is bulk modulus of the fluid (Pa), E is Young's modulus of the pipe (Pa), D is internal diameter of the pipe (m), e is wall thickness of the pipe (m), and ν is kinematic viscosity of the fluid (m^2/s).

Note that in the literature on hydraulic transients, the water-hammer equations are usually written in terms of hydraulic head H, but for convenience we have substituted the hydraulic head with $p=\rho gH$ in the water-hammer equations. If $p_w(z,t)$ is eliminated from Eqs. 1 and 2, one obtains

$$\frac{\partial^2 q_w(z,t)}{\partial z^2}-\frac{1}{a^2}\frac{\partial^2 q_w(z,t)}{\partial t^2}-\frac{R}{a^2}\frac{\partial q_w(z,t)}{\partial t}=0. \quad \ldots\ldots\ldots (3)$$

Eq. 3 is written in the Laplace domain, with $\mathcal{Q}_{wh}(s)$ and $\mathcal{Q}_{bh}(s)$ as the Laplace transforms of $q_{wh}(t)$ and $q_{bh}(t)$, as

$$\frac{\partial^2 \mathcal{Q}_w(z,s)}{\partial z^2}-\left(\frac{s^2}{a^2}+\frac{Rs}{a^2}\right)\mathcal{Q}_w(z,s)+\left(\frac{s}{a^2}+\frac{R}{a^2}\right)q_w(z,0)+\frac{1}{a^2}\frac{\partial q_w(z,0)}{\partial t}=0. \quad \ldots\ldots\ldots\ldots\ldots (4)$$

It is assumed that the well does not produce fluid at time $t\le 0$; i.e., that

$$q_w(z,0)=0,\ \frac{\partial q_w(z,0)}{\partial t}=0,\ 0\le z\le L_w, \quad \ldots\ldots\ldots (5)$$

where L_w is the well length. Applying the initial conditions of Eq. 5 in Eq. 4 and solving the equation lead to the solution

$$\mathcal{Q}_w(z,s)=M_1\sinh\xi z+M_2\cosh\xi z, \quad \ldots\ldots\ldots\ldots (6)$$

where

$$\xi^2=\frac{s^2}{a^2}+\frac{Rs}{a^2}, \quad \ldots\ldots\ldots\ldots\ldots\ldots (7)$$

and M_1 and M_2 are two unknown constants. Furthermore, if Eq. 1 is transformed into the Laplace domain and Eq. 6 is substituted into it, we obtain

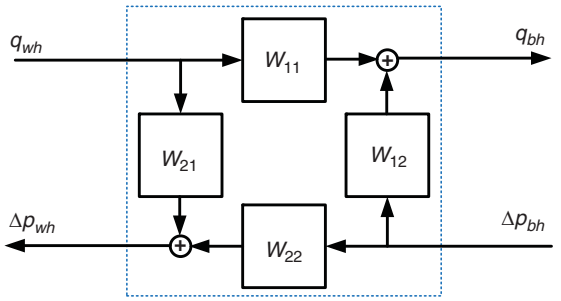

Fig. 2—Causal structure of the single-phase model, showing the relationships between inputs and outputs.

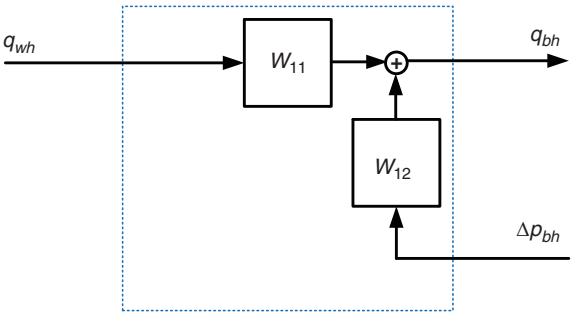

Fig. 3—Causal structure of the WBS model, showing the relationships between inputs and outputs.

$$\mathcal{P}_w(z,s)=\frac{-\rho a^2}{As}\xi(M_1\cosh\xi z+M_2\sinh\xi z)+\frac{p_w(z,0)}{s}, \quad \ldots\ldots\ldots\ldots\ldots\ldots (8)$$

where the last term is zero. Two boundary conditions are required to find M_1 and M_2. At each side of the pipe, either q or p can be specified. For example, in a well test, the choke controls the flow rate at the wellhead and the reservoir response determines the pressure at the bottom of the hole; therefore, $q_{wh}(t)$ and $p_{bh}(t)$ are taken as the boundary conditions. Finally, solving Eqs. 6 and 8 together gives

$$\begin{bmatrix}\mathcal{Q}_{bh}(s)\\ \mathcal{P}_{wh}(s)\end{bmatrix}=\mathbb{W}\begin{bmatrix}\mathcal{Q}_{wh}(s)\\ \mathcal{P}_{bh}(s)\end{bmatrix}, \quad \ldots\ldots\ldots\ldots\ldots\ldots (9)$$

in which the 2×2 matrix $\mathbb{W}$ is given by

$$\mathbb{W}(s)=\begin{bmatrix}W_{11} & W_{12}\\ W_{21} & W_{22}\end{bmatrix}=\begin{bmatrix}1/\cosh\xi L_w & -(sA/\rho\xi a^2)\tanh\xi L_w\\ (\rho\xi a^2/sA)\tanh\xi L_w & 1/\cosh\xi L_w\end{bmatrix}. \quad \ldots\ldots\ldots\ldots\ldots\ldots (10)$$

These four transfer functions, or filters, describe the full dynamic behavior of the flow of a slightly compressible single-phase liquid in a vertical well. **Fig. 2** represents the causal structure of Eq. 9 and illustrates how the inputs and outputs are connected. For example, the output $q_{bh}(t)$ is the sum of input $q_{wh}(t)$, filtered by W_{11}, and input $p_{bh}(t)$, filtered by W_{12}.

WBS Model. In practice, the assumption of single-phase liquid flow is only applicable to water-injection wells because in nearly all producing wells two-phase (gas/liquid) flow occurs. The analytical model for single-phase liquid flow, as derived previously, is then no longer applicable. In the PTA literature, the concept of WBS is used to model the dynamic effects after shut-in of a production well. In that case, a single WBS coefficient, C_s, describes the effect of wellbore-fluid compression on the well-flow rate q_{WBS} as

$$q_{\mathrm{WBS}(t)}=C_s\frac{\mathrm{d}p_{bh}(t)}{\mathrm{d}t}. \quad \ldots\ldots\ldots\ldots\ldots\ldots (11)$$

The mass-balance equation for the wellbore now becomes

$$q_{wh}(t)=q_{bh}(t)+C_s\frac{\mathrm{d}p_{bh}(t)}{\mathrm{d}t}, \quad \ldots\ldots\ldots\ldots\ldots\ldots (12)$$

which can be transformed into the Laplace domain as

$$\mathcal{Q}_{bh}(s)=\mathcal{Q}_{wh}(s)-C_s s\mathcal{P}_{bh}(s)+C_s p_{bh}(0), \quad \ldots\ldots\ldots (13)$$

where the last term is zero. Hence, the causal structure of Eq. 13 is illustrated in **Fig. 3,** where

$$W_{11}=1, \quad \ldots\ldots\ldots\ldots\ldots\ldots (14)$$

$$W_{12}=-C_s s. \quad \ldots\ldots\ldots\ldots\ldots\ldots (15)$$

Because in the WBS model only the mass-conservation equation is used, only two transfer functions appear in the causal structure.

Modeling the Fluid Flow in the Reservoir. Consider a circular reservoir with flow rate $q_{sf}(t)$ and pressure $p_{sf}(t)$ at the sandface of the well (Fig. 1). Recall that throughout this study we assume that all flow rates and pressures $q_x(t)$ and $p_x(t)$, with x representing an arbitrary subscript, are flow-rate and pressure differences with respect to the steady-state condition. It is assumed that an aquifer supports the reservoir with rate $q_e(t)$ and pressure $p_e(t)$ at the outer boundary; i.e., at $r=r_e$. In this homogeneous reservoir with single-phase, slightly compressible fluid, the radial flow rate $q_r(r,t)$ and pressure $p_r(r,t)$ at radial distance r from the symmetry axis satisfy the diffusivity equation and Darcy's law as

$$\frac{1}{r}\frac{\partial}{\partial r}r\frac{\partial p_r(r,t)}{\partial r}=\frac{1}{\eta}\frac{\partial p_r(r,t)}{\partial t}, \quad \ldots\ldots\ldots\ldots\ldots\ldots (16)$$

$$q_r(r,t)=-\frac{2\pi rkh}{\mu}\frac{\partial p_r(r,t)(t)}{\partial r}, \quad \ldots\ldots\ldots\ldots\ldots\ldots (17)$$

where $\eta=k/\phi\mu c_t$ is hydraulic diffusivity (1/s), C_t is total compressibility (1/Pa), k is absolute permeability (md), ϕ is porosity, μ is fluid viscosity (Pa·s), and h is reservoir thickness (m).

The initial condition can be expressed as

$$p_r(r,0)=0, \ \ r_w\le r\le r_e. \quad \ldots\ldots\ldots\ldots\ldots\ldots (18)$$

Note that p_r represents the difference with respect to the steady-state condition. If $\mathcal{P}_r(r,s)$ and $\mathcal{Q}_r(r,s)$ are the Laplace transforms of $p_r(r,t)$ and $q_r(r,t)$, we can write Eq. 16 in the Laplace domain as

$$r\frac{\partial}{\partial r}r\frac{\partial\mathcal{P}_r(r,s)}{\partial r}=\frac{s}{\eta}r^2\mathcal{P}_r(r,s). \quad \ldots\ldots\ldots\ldots\ldots\ldots (19)$$

Solving this ordinary-differential equation in the radial coordinate leads to the solution

$$\mathcal{P}_r(r,s)=M_1I_0\left(\sqrt{\frac{s}{\eta}}r\right)+M_2K_0\left(\sqrt{\frac{s}{\eta}}r\right), \quad \ldots\ldots\ldots (20)$$

in which M_1 and M_2 are two arbitrary coefficients. To find their magnitudes, we invoke the Laplace transform of Eq. 17:

$$\mathcal{Q}_r(r,s)=-\frac{2\pi kh}{\mu}\left[M_1r\sqrt{\frac{s}{\eta}}I_1\left(\sqrt{\frac{s}{\eta}}r\right)-M_2r\sqrt{\frac{s}{\eta}}K_1\left(\sqrt{\frac{s}{\eta}}r\right)\right], \quad \ldots\ldots\ldots\ldots\ldots\ldots (21)$$

and choose two boundary conditions, which, at each boundary, can be specified in terms of either p or q. We assume that at the sandface the flow rate $q_{sf}(t)$ is imposed, and at the outer boundary

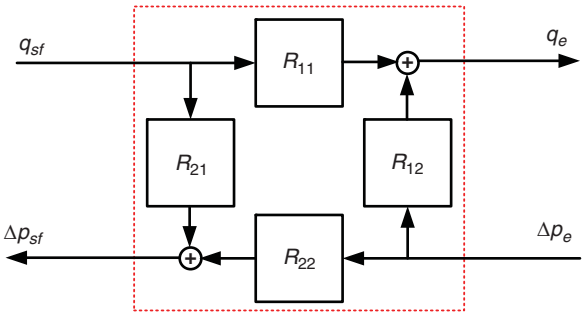

Fig. 4—Causal representation of the reservoir model, showing the relationship between inputs and outputs.

the pressure $p_e(t)$. By solving Eqs. 20 and 21, the dynamical behavior of the reservoir is then derived as

$$\begin{bmatrix} \mathrm{Q}_e(s) \\ \mathrm{P}_{sf}(s) \end{bmatrix} = \mathbb{R} \begin{bmatrix} \mathrm{Q}_{sf}(s) \\ \mathrm{P}_e(s) \end{bmatrix}, \quad \ldots\ldots\ldots\ldots\ldots\ldots\ldots\ldots (22)$$

where $\mathbb{R}$ is a 2×2 matrix with

$$R_{11}(s) = \frac{r_e}{r_w} \frac{I_1\left(r_e\sqrt{\frac{s}{\eta}}\right)K_0\left(r_e\sqrt{\frac{s}{\eta}}\right) + I_0\left(r_e\sqrt{\frac{s}{\eta}}\right)K_1\left(r_e\sqrt{\frac{s}{\eta}}\right)}{I_0\left(r_e\sqrt{\frac{s}{\eta}}\right)K_1\left(r_w\sqrt{\frac{s}{\eta}}\right) + I_1\left(r_w\sqrt{\frac{s}{\eta}}\right)K_0\left(r_e\sqrt{\frac{s}{\eta}}\right)}, \quad \ldots\ldots\ldots\ldots\ldots\ldots\ldots\ldots (23)$$

$$R_{12}(s) = \frac{2\pi kh}{\mu} \times r_e\sqrt{\frac{s}{\eta}} \frac{I_1\left(r_w\sqrt{\frac{s}{\eta}}\right)K_1\left(r_e\sqrt{\frac{s}{\eta}}\right) - I_1\left(r_e\sqrt{\frac{s}{\eta}}\right)K_1\left(r_w\sqrt{\frac{s}{\eta}}\right)}{I_0\left(r_e\sqrt{\frac{s}{\eta}}\right)K_1\left(r_w\sqrt{\frac{s}{\eta}}\right) + I_1\left(r_w\sqrt{\frac{s}{\eta}}\right)K_0\left(r_e\sqrt{\frac{s}{\eta}}\right)}, \quad \ldots\ldots\ldots\ldots\ldots\ldots\ldots\ldots (24)$$

$$R_{21}(s) = \frac{\mu}{2\pi kh r_w\sqrt{\frac{s}{\eta}}} \times \frac{I_0\left(r_e\sqrt{\frac{s}{\eta}}\right)K_0\left(r_w\sqrt{\frac{s}{\eta}}\right) - I_0\left(r_w\sqrt{\frac{s}{\eta}}\right)K_0\left(r_e\sqrt{\frac{s}{\eta}}\right)}{I_0\left(r_e\sqrt{\frac{s}{\eta}}\right)K_1\left(r_w\sqrt{\frac{s}{\eta}}\right) + I_1\left(r_w\sqrt{\frac{s}{\eta}}\right)K_0\left(r_e\sqrt{\frac{s}{\eta}}\right)}, \quad \ldots\ldots\ldots\ldots\ldots\ldots\ldots\ldots (25)$$

$$R_{22}(s) = \frac{I_0\left(r_w\sqrt{\frac{s}{\eta}}\right)K_1\left(r_w\sqrt{\frac{s}{\eta}}\right) + I_1\left(r_w\sqrt{\frac{s}{\eta}}\right)K_0\left(r_w\sqrt{\frac{s}{\eta}}\right)}{I_0\left(r_e\sqrt{\frac{s}{\eta}}\right)K_1\left(r_w\sqrt{\frac{s}{\eta}}\right) + I_1\left(r_w\sqrt{\frac{s}{\eta}}\right)K_0\left(r_e\sqrt{\frac{s}{\eta}}\right)}. \quad \ldots\ldots\ldots\ldots\ldots\ldots\ldots\ldots (26)$$

As illustrated in **Fig. 4,** each output is connected to two inputs, and the causal structure of the flow dynamics of the reservoir is therefore identical to that of the single-phase wellbore. The transfer function of interest in PTA is $R_{21}(s)$, which describes the effect of $q_{sf}(t)$ on $p_{sf}(t)$. Adding a skin factor S_r to Eq. 25 gives

$$R_{21,S_r} = R_{21} + \frac{\mu S_r}{2\pi kh}. \quad \ldots\ldots\ldots\ldots\ldots\ldots\ldots\ldots (27)$$

To reduce notation complexity, we use R_{21} instead of R_{21,S_r} throughout the study.

Bilaterally Coupling the Wellbore and Reservoir Models. We have represented the reservoir and the wellbore as linear systems with two bilaterally coupled ports—i.e., with two inputs, two outputs, and four transfer functions—to describe the complete input/output relationships and causal structure. At the boundary, power is exchanged as a result of the mutual interaction between the system and its environment. Power can be represented as the product of a flow variable and a potential variable, which in our case are $q(t)$ and $p(t)$, respectively. In the interaction at the boundary, one variable is imposed on the system by the environment and, consequently, the other is determined by the system response (Bosgra 2009). After deriving the individual models of the wellbore and the reservoir, a well-test-response model is constructed through bilateral coupling. Note that in the case of a WBS model, which does not contain W_{21} and W_{22}, the bilateral coupling of the models is still possible because the wellbore has the two required connections at the sandface side. To complete the well-test-response model, the wellhead side of the wellbore and the outer-edge side of the reservoir are connected to a flow and a potential source, respectively **(Figs. 5 and 6).**

The networks in Figs. 5 and 6 illustrate that the bottomhole variables are internal variables that are influenced by the dynamics of both the wellbore and the reservoir. As mentioned previously, in PTA the transfer function $R_{21}(s)$ has to be identified. If only the network elements that directly influence R_{21} are kept, a reduced model is obtained that contains a feedback loop from p_{bh} to q_{bh} **(Fig. 7).** This reduced model clearly shows how the reservoir and wellbore dynamics influence the bottomhole variables. Taking into account the feedback loop between the internal variables, the network equations can be written as

$$\mathcal{Q}_{bh}(s) = W_{11}(s)S(s)\mathcal{Q}_{wh}(s) + R_{22}(s)W_{12}(s)S(s)\mathcal{P}_e(s), \quad \ldots\ldots\ldots\ldots\ldots\ldots\ldots\ldots (28)$$

$$\mathcal{P}_{bh}(s) = R_{21}(s)W_{11}(s)S(s)\mathcal{Q}_{wh}(s) + R_{22}(s)S(s)\mathcal{P}_e(s), \quad \ldots\ldots\ldots\ldots\ldots\ldots\ldots\ldots (29)$$

where the sensitivity function is defined as

$$S(s) = 1/[1 - R_{21}(s)W_{12}(s)]. \quad \ldots\ldots\ldots\ldots\ldots\ldots\ldots\ldots (30)$$

These relationships reveal how the inputs q_{wh} and p_e affect the bottomhole-flow rate and pressure. Note that the structure of the

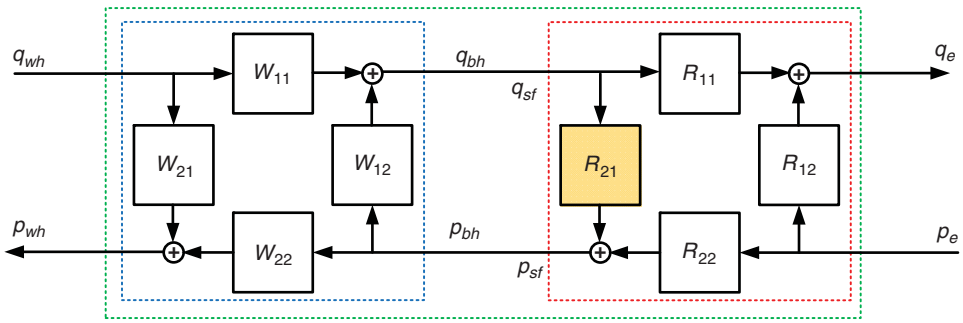

Fig. 5—Bilateral coupling of single-phase wellbore and reservoir models.

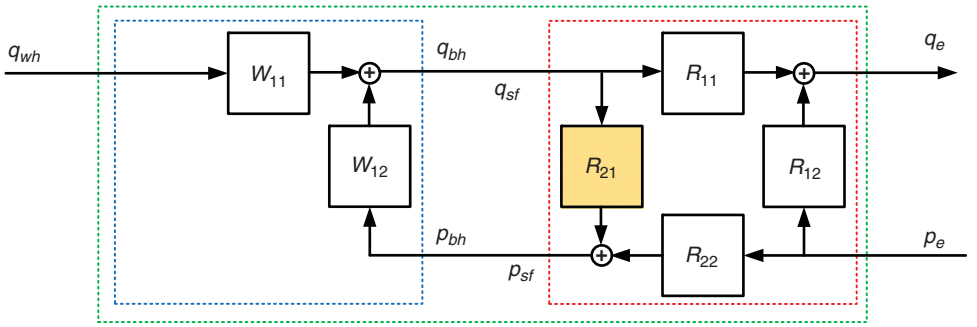

Fig. 6—Bilateral coupling of WBS and reservoir models.

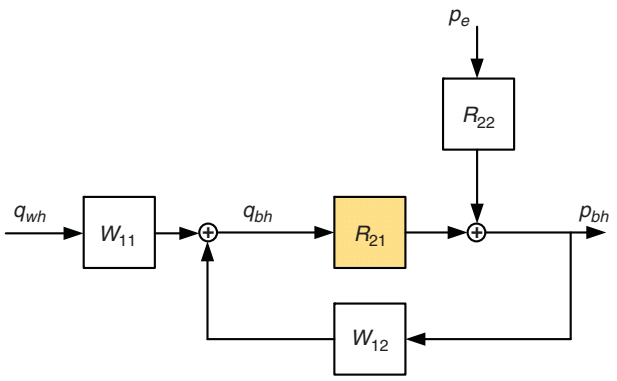

Fig. 7—Influential elements (white) of the bilaterally coupled wellbore/reservoir network for $R_{21}(s)$ (yellow).

reduced model does not depend on whether the wellbore is represented with a single-phase or a WBS model.

Simulation shows that for typical wellbore and reservoir properties as listed in **Table 1,** the contribution of P_e, filtered with R_{22}, is negligible in the final value of p_{bh} for the first 70 days. Thus, we remove this input route from the network. **Fig. 8** shows the final simplified network, which has an output-feedback structure. For this simplified network, Eqs. 28 and 29 reduce to

$$\mathcal{Q}_{bh}(s) = W_{11}(s)S(s)\mathcal{Q}_{wh}(s), \quad \ldots\ldots\ldots\ldots\ldots\ldots (31)$$

$$\mathcal{P}_{bh}(s) = R_{21}(s)W_{11}(s)S(s)\mathcal{Q}_{wh}(s). \quad \ldots\ldots\ldots\ldots\ldots (32)$$

To compare the derived structure to those described in the PTA literature, the transfer functions W_{11} and W_{12} in Eqs. 31 and 32 are replaced with those of the WBS wellbore model: Eqs. 14 and 15. This substitution leads to the expressions for bottomhole-flow rate and pressure as used in conventional PTA (Kuchuk 1990). This illustrates that the model presented in this study is just a more-general description of the conventional representation of a well-test-response model. However, the causal structure of the model clearly discriminates the wellbore and reservoir effects on the bottomhole variables and shows the presence of a feedback mechanism between the variables. As will be described later in this study, this feedback has major consequences for the selection of a suitable identification procedure.

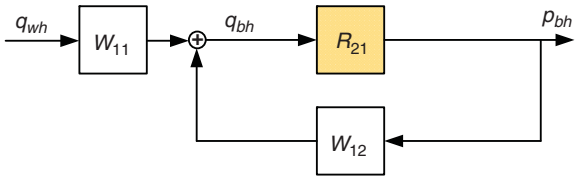

Fig. 8—Influential elements (white) of the bilaterally coupled wellbore/reservoir network for $R_{21}(s)$ (yellow) after simplification and removing the input p_e.

Model Properties	SI Units
Reservoir boundary (r_e)	2000 m
Well radius (r_w)	0.1 m
Reservoir thickness (H)	50 m
Pipe internal diameter (D)	0.1 m
Pipe-wall thickness (e)	16×10^{-3} m
Well length (L)	2000 m
Permeability (k)	2×10^{-13} m^2
Porosity (ϕ)	0.2
Dynamic viscosity (μ)	0.01 Pa·s
Kinematic viscosity ($\mathcal{V}$)	1.11×10^{-5} m^2/s
Total compressibility (C_t)	7.25×10^{-9} 1/Pa
Bulk modulus of the fluid (K)	1.5×10^{9} Pa
Fluid density (ρ)	900 kg/m^3
Young's modulus of the pipe (E)	200×10^{9} Pa
WBS coefficient (C_s)	4.58×10^{-8} m^3/Pa
Skin (S_r)	0

Table 1—Wellbore and reservoir properties.

Analysis of Wellbore and Reservoir Models. In this subsection, we analyze the dynamic behavior of the simplified network for property values listed in Table 1. **Figs. 9 and 10** display the magnitudes (amplitudes) of the frequency responses for the single-

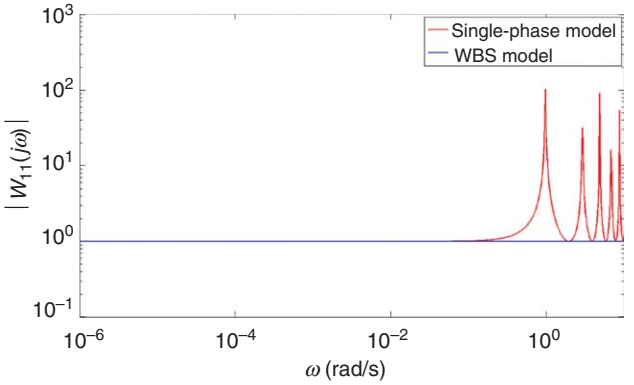

Fig. 9—Magnitude of the frequency response of $W_{11}(j\omega)$; (red) single-phase model, (blue) WBS model.

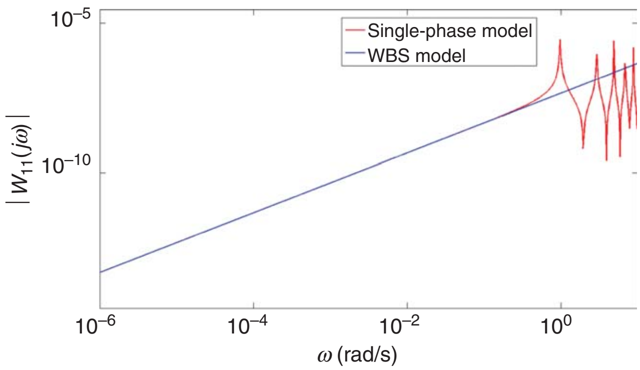

Fig. 10—Magnitude of the frequency response of $W_{12}(j\omega)$; (red) single-phase model, (blue) WBS model.

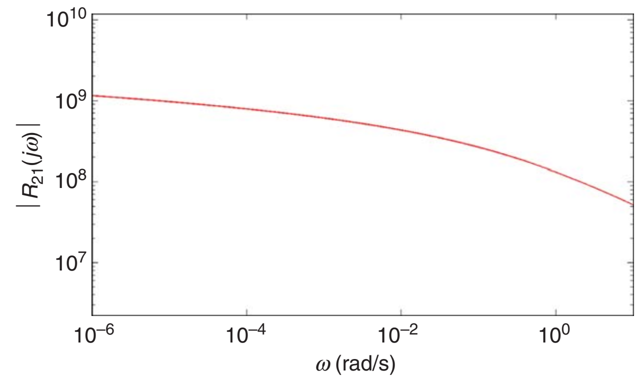

Fig. 11—Magnitude of the frequency response of $R_{21}(j\omega)$.

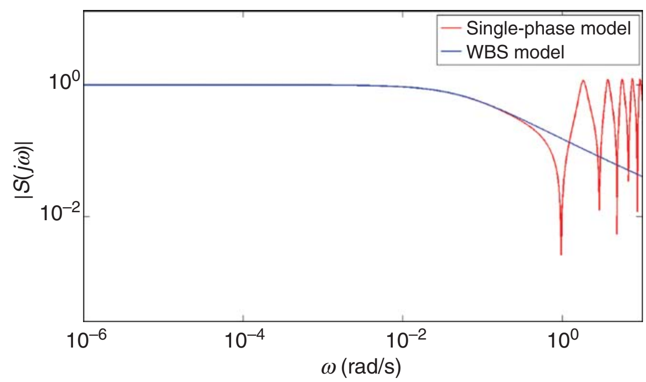

Fig. 12—Magnitude of the frequency response of sensitivity function $S(j\omega)$.

phase and WBS models. The single-phase response shows many resonant peaks at high frequencies, which are absent in the WBS response. These resonances correspond to the frequencies at which pressure waves travel up and down the liquid column. The smooth-frequency response of the WBS model does not show any resonances because the WBS model only represents the effect of compressibility and not of inertia. In this case, W_{12} shows the storage effect, represented by C_s, as the slope of the blue line. Note that at low frequencies, both models display an identical frequency response. This equality can be used to calculate the WBS coefficient C_s in terms of the single-phase-flow parameters. If the transfer functions of the single-phase model are considered for $\omega \to 0$ and then compared with those of the WBS model, it follows that

$$C_s = AL_w/\rho a^2. \quad (33)$$

The frequency response of the reservoir-transfer function, R_{21}, has been depicted in **Fig. 11.** It shows a smooth- and low-frequency dominant behavior that is the characteristic of a diffusive system.

The combined effect of the transfer functions R_{21} and W_{12} is present in the feedback loop in Fig. 8. It follows from the definition of the sensitivity function in Eq. 30 that for values of $S(s)$ close to unity the feedback does not affect the system; otherwise, it influences the entire dynamic behavior of the system. For the parameter values in our example, the feedback effect is negligible at less than approximately 10^{-2} rad/s **(Fig. 12).** For frequencies greater than 10^{-2} rad/s, the blue curve displays a downward trend, whereas the red curve starts to oscillate.

A different way to illustrate this effect is through simulating a step response of the network for both cases **(Fig. 13).** The step response of q_{bh} for the single-phase model shows spikes and an oscillatory behavior at early times, whereas the response for the WBS model shows a smooth behavior. At later times, both systems behave increasingly similarly and the dynamic effect of the feedback vanishes. The early spikes of the single-phase model

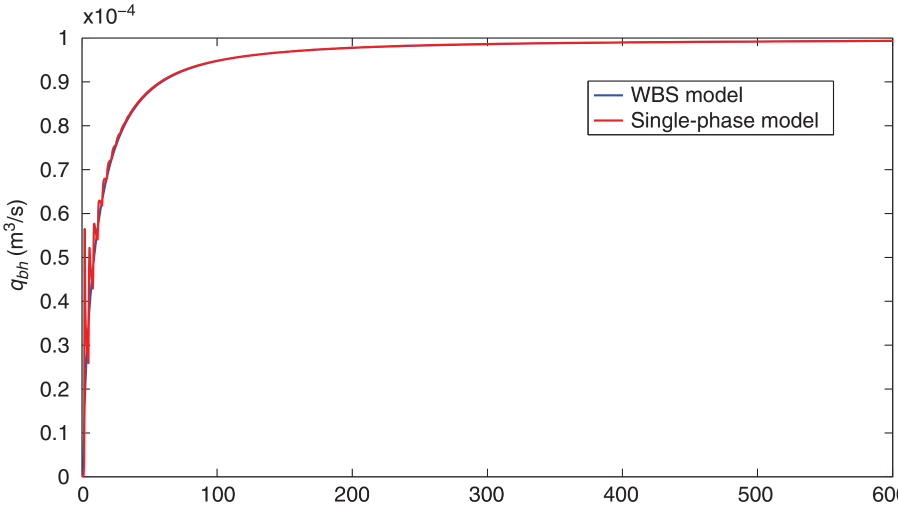

Fig. 13—Bottomhole flow rate $q_{bh}(t)$ for a step-rate change in the wellhead flow rate $q_{wh}(t)$ for the single-phase and the WBS models.

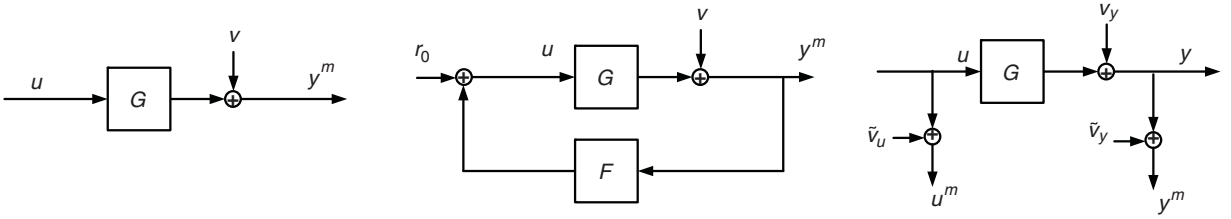

Fig. 14—Three SI configurations: (left) open-loop case, (middle) closed-loop case, (right) EIV case.

result from pressure waves in the well that quickly die out because of strong damping in the reservoir.

Model Identification and Parameter Estimation

System Identification (SI). SI is the process of estimating a mathematical model of a physical system by use of experimental data that may be contaminated by unknown disturbances (process noise) and sensor noise. A brief introduction to SI concepts and techniques is given in Appendix A. A complete overview can be found in Ljung (1999). Usually, SI techniques are applied to data that are discrete-time signals, in which case a discrete-time approximation of the physical system is identified. The output of a discrete-time dynamical system G_0 that is excited by an input $u(k)$ is

$$y(k) = G_0\left(q^{-1}\right)u(k) + H_0\left(q^{-1}\right)e(k);\ k = 1, \ldots, N, \quad \ldots\ (34)$$

where the symbol q^{-1} is the shift operator—i.e., $q^{-1}u(k) = u(k-1)$, in which k is discrete time—$G_0(q^{-1})$ is the discrete-time transfer function of the physical system, $e(k)$ is a white-noise signal, and H_0e (H_0 is monic and stable transfer function) represents both sensor noise and disturbances. The goal of SI is to obtain estimates of the transfer functions G_0 and H_0 of the data-generating system on the basis of the measured data $[u(k), y(k)]_{k=1,\cdots,N}$.

A powerful SI method is the prediction-error method (PEM), in which a one-step-ahead prediction error for the system is defined as (see Appendix B for details)

$$\varepsilon(k,\theta) = H^{-1}\left(q^{-1},\theta\right)[y(k) - G\left(q^{-1},\theta\right)u(k)]. \quad \ldots\ldots\ (35)$$

The parameterized transfer functions $G(q^{-1},\theta)$ and $H(q^{-1},\theta)$ are estimated by minimizing the average-squared-prediction error:

$$\hat{\theta}_N = \arg\min_{\theta} \frac{1}{N}\sum_{k=1}^{N} \varepsilon^2(k,\theta), \quad \ldots\ldots\ldots\ldots\ (36)$$

where $\theta \in \mathcal{R}^d$ is a real-valued parameter vector. The parameterization of models G and H depends on the model structure, which must be chosen before applying Eq. 35. There are several black-box model structures that can be used for fitting the data and estimating the system and noise models. For example, in the Box-Jenkins (BJ) model structure (Box et al. 1994), the system and noise models are independently parameterized as $G(q^{-1},\theta) = B(q^{-1},\theta)/F(q^{-1},\theta)$ and $H(q^{-1},\theta) = C(q^{-1},\theta)/D(q^{-1},\theta)$, where B, C, D, and F are polynomials in the shift operator q^{-1}. For the simpler auto-regressive-external-input model structure, $C = I$ and $D = F$, and for the output-error model structure, $H = I$. After choosing the model structure and substituting the corresponding equations into Eq. 35, a linear- or nonlinear-regression problem has to be solved to obtain the parameter vector θ_N. For example, use of the BJ model structure leads to a one-step-ahead prediction error:

$$\varepsilon(k,\theta) = \frac{\left(1 + \sum_{m=1}^{n_c} c_m q^{-m}\right)}{\left(1 + \sum_{m=1}^{n_d} d_m q^{-m}\right)} \times \left[y(k) - \frac{\sum_{m=1}^{n_b} b_m q^{-m}}{\left(1 + \sum_{m=1}^{n_f} f_m q^{-m}\right)} u(k)\right], \quad \ldots\ (37)$$

and consequently a nonlinear optimization has to be solved to obtain the parameter vector $\hat{\theta}_N$ of the polynomials. The estimated parameter vector is a random variable with normal distribution,

$$\hat{\theta} \in \mathcal{N}\left(\theta_0, P\hat{\theta}\right), \quad \ldots\ldots\ldots\ldots\ (38)$$

where $P_{\hat{\theta}}$ is the estimated covariance matrix and θ_0 is the true parameter vector. An important property of the covariance matrix is that it asymptotically approaches zero as the number of measurements approaches infinity; i.e., for experiments with an infinite number of measurements, $\hat{\theta}$ approaches θ_0 asymptotically.

To validate the identified model, different statistics-based tests such as residual tests can be performed. For example, by use of $P_{\hat{\theta}}$, the cross-correlation test that will be used in this study is such that one can conclude with 99% confidence that there is no evidence in the data that the model is wrong.

To implement the PEM, two important prerequisites must be fulfilled: First, the input signal u has to be persistently exciting of sufficiently high-order, which simply means that it has to be "variable enough" to excite all relevant dynamics in the system; second, the noise term in the output must be uncorrelated with the input signal u. The second condition can be checked by assessing the causal structure of the system. For example, the left-hand side **Fig. 14** shows that an open-loop structure fulfills this condition. In this configuration, the system is excited by a reference signal u and there is no link and therefore no correlation between u and v. For systems operating under the effects of a feedback loop, such as a system with a controller, this condition is violated because the feedback mechanism transfers the effects of the noise to the input of the system (Fig. 14, middle). In this case, the input u is a combination of the reference signal r and the filtered output, which has the noise effect in itself. The reference signal comes from the environment and affects the system, but does not receive any effect from the system. To identify such systems, so-called closed-loop SI methods have been developed (Van den Hof 1998). Another important case in which it is impossible to apply PEM directly is when the measured input and output both contain noise (Fig. 14, right). This case, in which a noise-free input signal is not available, is called an errors-in-variables (EIV) problem. A complete review of this problem has been presented in Söderström (2007). EIV problems usually suffer from lack of identifiability. However, under special assumptions about the noise and the input signal, the identifiability issue can be resolved.

Measurement Setup. We assume that during a well test in the production system depicted in Fig. 5, one manipulates the surface flow rate q_{wh}, on the basis of a planned schedule, and measures the downhole flow rate q^m_{bh} and pressure p^m_{bh}. We assume that measurements are contaminated with different unknown disturbances, and in addition sensor noise is present. Both of these effects can be modeled as a stationary stochastic process; the disturbances act as internal inputs to the network and affect the system, whereas the sensor noise just influences the measurement data. We denote the disturbances and sensor noise with $v(t)$ and $\tilde{v}(t)$, respectively. **Fig. 15** shows the network in which the measurement devices have been indicated and both disturbance and sensor noise have been taken into account.

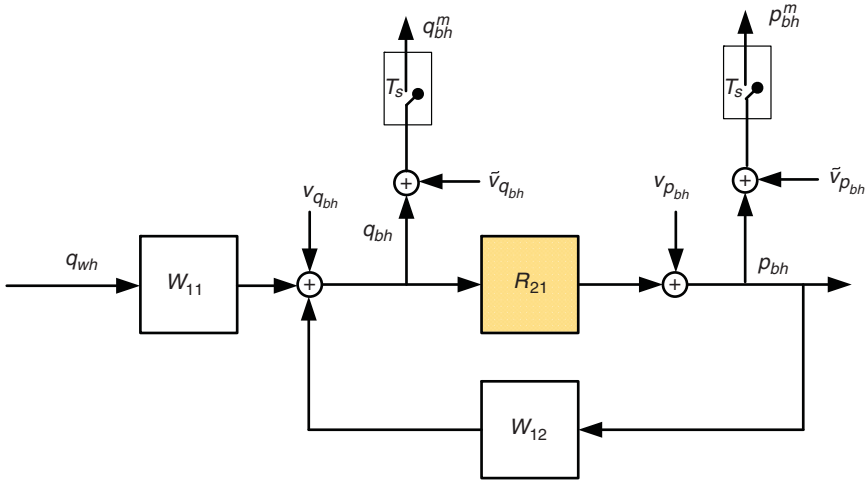

Fig. 15—Data-generating system including disturbances and sensor noise.

Because the measurement devices sample the continuous variables at periodic intervals of T_s in seconds, it is convenient to use discrete-time notation to describe the system equations:

$$q^m_{bh}(k) = (W_{11}S)^d\left(q^{-1}\right)q_{wh}(k) + w_q(k), \quad \ldots\ldots\ldots\ldots (39)$$

$$p^m_{bh}(k) = (R_{21}W_{11}S)^d\left(q^{-1}\right)q_{wh}(k) + w_p(k), \quad \ldots\ldots\ldots (40)$$

where the superscript d indicates discrete time and

$$w_q(k) = S^d\left(q^{-1}\right)v_{q_{bh}}(k) + (W_{12}S)^d\left(q^{-1}\right)v_{p_{bh}}(k) + \tilde{v}_{p_{bh}}(k), \quad \ldots\ldots\ldots\ldots\ldots\ldots (41)$$

$$w_p(k) = (R_{21}S)^d\left(q^{-1}\right)v_{q_{bh}}(k) + S^d\left(q^{-1}\right)^d v_{p_{bh}}(k) + \tilde{v}_{p_{bh}}(k), \quad \ldots\ldots\ldots\ldots\ldots\ldots (42)$$

are the noise terms.

To identify the reservoir model from the bottomhole measurements, a closed-loop SI method must be used, but because q^m_{bh} and p^m_{bh} contain sensor noise, a so-called direct closed-loop SI method cannot be applied (Ljung 1999). The identification problem for this case is known as an EIV identification problem in a closed-loop configuration. Söderström et al. (2013) have investigated this problem and concluded that the system under such conditions is not identifiable merely by use of noisy input and output—i.e., measured bottomhole flow rate and pressure—but is identifiable if a so-called reference signal is available. A reference signal defines the set-point that the system has to follow (i.e., it is a control signal), and has to enter the system from outside the loop. Thus, in our system $q_{wh}(t)$ can be considered as the reference signal. In Appendix C, a spectral analysis of the well-test problem has been presented to illustrate how the use of q_{wh} as a reference signal leads to the identifiability of R^d_{21}. The availability of a reference signal makes it possible to use an indirect closed-loop SI technique, known as a two-stage (TS) method.

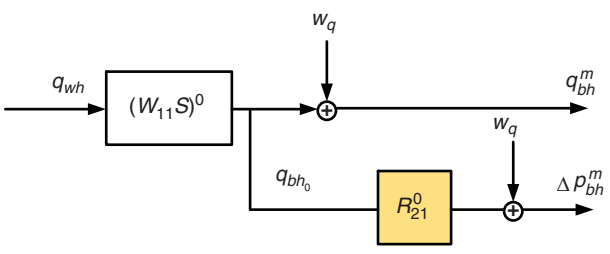

Fig. 16—The TS method breaks down the EIV problem into two subsequent open-loop identification problems.

TS Closed-Loop Identification. The TS method subdivides the problem in two successive open-loop identification problems (Van den Hof and Schrama 1993). The idea behind the method is to first estimate the noise-free input of the system and then use this input for identification of the system. In the first stage, the transfer function $G_{fs}(q^{-1},\theta)$, approximating $(W_{11}S)^d(q^{-1})$, is identified by use of measurements of q_{wh} and q^m_{bh} on the basis of Eq. 39. Then, this model is used to reconstruct the noise-free bottomhole flow-rate signal $\hat{q}_{bh_0}$:

$$\hat{q}_{bh_0}(k) = G_{fs}\left(q^{-1},\hat{\theta}_N\right)q_{wh}(k);\ k = 1,\ldots N. \quad \ldots\ldots\ldots (43)$$

In the simulated $\hat{q}_{bh0}(k)$, there is no longer any effect from the stochastic-noise signal $w_q(k)$ because it has been removed in the identification. Thereafter, a second identification is performed by use of $\hat{q}_{bh_0}$ and p^m_{bh} on the basis of Eq. 40 to identify the $R^d_{21}\left(q^{-1},\hat{\theta}_N\right)$; **Fig. 16** illustrates the two consecutive open-loop identification steps.

Physical-Parameter Estimation

To complete the pressure-transient-analysis procedure, the physical parameters of the reservoir have to be estimated by use of the identified model. To perform this step, we compare the frequency response of the identified model to the frequency response of one or more analytical reservoir models. These analytical models can be derived by solving the partial-differential equations for single-phase (diffusive) flow in the reservoir in the Laplace domain. The solution of these equations results in an irrational reservoir model such as $R_{21}(s,\beta)$ in Eq. 25, where β is a vector of relevant physical parameters. Frequently used parameters in well testing are average permeability k and skin factor S_r. In the identification step, this analytical model has been approximated with a finite-order discrete-time dynamical model—i.e., $R^d_{21}\left(q^{-1},\hat{\theta}_N\right)$—on the basis of the bottomhole measurements.

The reservoir parameter β can be estimated as the minimizer of a suitable difference measure between the parameterized reservoir model $R_{21}(s,\beta)$ and the identified model $R^d_{21}\left(q^{-1},\hat{\theta}_N\right)$. However, two important issues have to be addressed before performing the minimization. First, the difference between the domains of the models should be resolved: The identified model is in the time domain, whereas the analytical solution is in the Laplace (complex) domain. Second, the difference between discrete-time and continuous-time models should be overcome. To address the first issue, the identified time-domain model can be simply transformed to the complex domain by substituting the shift operator q with z where z is a complex variable. Thus, $R^d_{21}\left(q^{-1},\hat{\theta}_N\right)$ is transformed to $R^d_{21}\left(z^{-1},\hat{\theta}_N\right)$. To overcome the

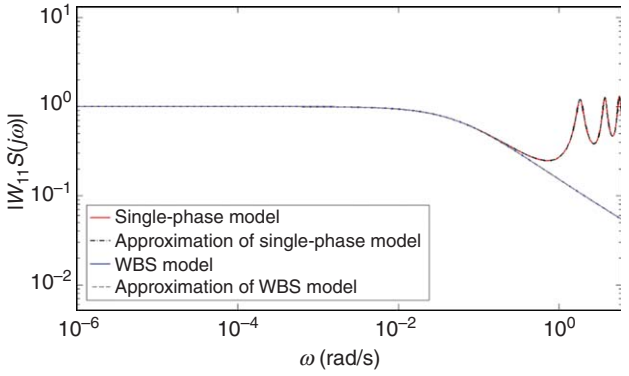

Fig. 17—Comparison between $W_{11}S(j\omega)$ and its VF approximation.

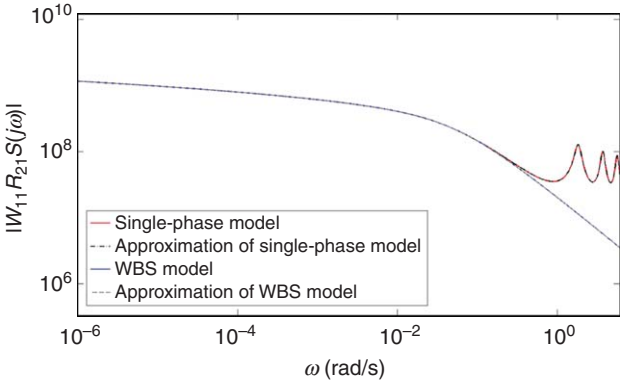

Fig. 18—Comparison between $W_{11}R_{21}S(j\omega)$ and its VF approximation.

second issue, a continuous-time approximation of the discrete-time model can be obtained by use of, for example, a zero-order-hold or a first-order-hold approximation of the intersample behavior for the discrete model. A more-efficient way, which is used in this study, is to transform both the discrete and continuous models from their respective complex domains (the Laplace and the z-domain) into the frequency domain and perform the parameter estimation in that domain. This transformation is obtained by simply substituting s with $j\omega$ and z with $e^{j\omega}$, where j is the imaginary unit. Thereafter, the comparison can be performed by use of

$$R_{21}(\beta, j\omega) \approx R^d{}_{21}\left(e^{j\omega}, \hat{\theta}_N\right), \quad \omega \in (\omega_L, \omega_H), \quad \ldots\ldots\ldots (44)$$

where the lower frequency ω_L cannot be lower than the frequency resolution of the input signal, and the upper frequency ω_H cannot be larger than half of the sampling frequency. Alternatively, the comparison may be performed in the Laplace domain (Bourgeois and Horne 1993). Note that, in theory, deconvolution could also be performed directly in the Laplace domain, but this would lead to incorrect results for measured data containing noise. An important element of our SI method is the removal of noise before the reservoir-model characterization and physical-parameter estimation. Because of the nature of the SI method this results in a time-domain model along with the statistical properties of the model derived from the stochastic part of the signal (i.e., the noise). The model and its statistical properties are easily transformed into the frequency domain for physical-parameter estimation. In addition, the statistical properties of the model provide the proper frequency range for the estimation. For a complete review of the signal and system properties in time and complex domains, we refer to Oppenheim et al. (1999).

The identified finite-order reservoir model is, generally, not equally accurate at all frequencies of this frequency range. In particular, the quality of the identified model is low at frequencies where the input signal q_{bh_0} does not exert enough excitation. The excitation levels at different frequencies can be calculated by computing the spectral density of the signal. Based on the calculated spectral density of the input signal, the frequency range (ω_L, ω_H) in Eq. 44 may have to be modified. This frequency range may also be chosen on the basis of the statistical properties of the identified model. The estimated covariance matrix $P\hat{\theta}$ is then used to estimate the covariance of the identified model $\mathrm{cov}[R^d_{21}\left(e^{j\omega}, \hat{\theta}\right)]$. The covariance can be plotted as a confidence bound around the frequency response of the identified model and used as a measure of the uncertainty of the identified model in different frequencies.

The physical-parameter-estimation problem can now be expressed as

$$\hat{\beta} = \frac{1}{M}\arg\min_{\beta}\sum_{m=1}^{M} \| R_{21}(\beta, j\omega_m) - R^d{}_{21}\left(e^{j\omega_m}, \hat{\theta}_N\right) \| W(\omega_m), \quad \ldots\ldots\ldots\ldots\ldots\ldots (45)$$

where $\omega_1 = \omega_L$, $\omega_M = \omega_H$, and M and $W(\omega_m)$ are tuning variables that specify the number of comparison points and the weighting function at those points, respectively.

Synthetic Examples

Simulation. To generate synthetic data for the case of a variable wellhead flow rate, Eqs. 31 and 32 can be used to simulate the network. Because these equations are in the Laplace domain, a numerical Laplace-inversion technique, such as the Stehfest algorithm, can be used (Stehfest 1970). However, the Stehfest algorithm is not suitable for the inversion of the solution of hyperbolic equations that display oscillatory behavior (Hassanzadeh and Pooladi-Darvish 2007). To handle this issue, we use discrete-time approximations of the transfer functions in the data-generating simulation model, which is a standard procedure in control engineering for simulating the response of a system. The transfer functions in Eqs. 10 and 25 are irrational functions of $\sqrt{s}$, and therefore the usual discretization schemes, such as Euler's method, cannot be applied straightforwardly. To circumvent this issue, first a rational continuous-time approximation of the original transfer function,

$$G(\sqrt{s}) \approx \frac{\sum_{k=0}^{M} b_k s^{-k}}{\left(1 + \sum_{k=1}^{N} a_k s^{-k}\right)}, \quad \ldots\ldots\ldots\ldots\ldots (46)$$

is required; in Eq. 46 the parameter vectors b and a are estimated by use of a suitable fitting algorithm. Several algorithms such as Pade's algorithm (Press et al. 2007) or series expansions are available for obtaining such an approximation, but we use the vector-fitting (VF) algorithm that can obtain a good fit over a large frequency range (Gustavsen and Semlyen 1999). In the VF algorithm the numerical values of the original irrational-transfer function are applied and a stable approximation of the original transfer function over the selected frequency range is computed. After obtaining the rational approximation, a suitable discretization scheme can be used to calculate the discrete-time-transfer function. In **Figs. 17 and 18,** the approximated transfer functions of $W_{11}R_{21}S$ and $W_{11}S$ are displayed. The approximations show a very-good fit with the original irrational-transfer function.

To simulate the well-test process, we assign a pseudorandom binary (PRB) flow-rate sequence with a magnitude of 1×10^{-4} m^3/s at the wellhead for a period of $T_{\mathrm{exp}} = 10^6$ seconds. PRB signals are often used as the input signal in identification experiments because they can be designed to generate a persistently exciting input. A limit on the flow-rate change is taken into account by letting the time period of the designed PRB signal be 3,600 seconds; i.e., the surface choke has to be in one state for at least 1 hour. It is assumed that the reservoir has been producing at steady-state conditions before the experiment is triggered, so the varying $q_{wh}(t)$ is applied on top of the steady-state-flow rate. Hence, the resulting bottomhole-rate and pressure responses are also deviations from the corresponding steady-state values.

Case No.	q_{wh}	Wellbore Model	w_q	w_p
Case 1	PRBS	Single-phase model	SNR = 24.5	SNR = 28.7
			$\sigma_{\tilde{y}} \approx \pm 5.9\times10^{-6}$ m^3/s	$\sigma_{w_p} \approx \pm$ 2460 Pa
Case 2	PRBS	WBS model	SNR = 21.9	SNR = 28.7
		$C_s = 4.58\times10^{-8}$ m^3/Pa	$\sigma_{w_q} \approx \pm 7.9\times10^{-6}$ m^3/s	$\sigma_{w_p} \approx \pm$ 2474 Pa
Case 3	PRBS	WBS model	SNR = 20.3	SNR = 27.8
		$C_s = 2.33\times10^{-6}$ m^3/Pa	$\sigma_{w_q} \approx \pm 7.1\times10^{-6}$ m^3/s	$\sigma_{w_q} \approx \pm$ 2184 Pa
Case 4	Random	WBS model	SNR = 14.4	SNR = 20.3
		$C_s = 2.33\times10^{-6}$ m^3/Pa	$\sigma_{w_q} \approx \pm 6.4\times10^{-6}$ m^3/s	$\sigma_{w_p} \approx \pm$ 2184 Pa
Case 5	PRBS	WBS model	SNR = 14.3	SNR = 18.1
		$C_s = 2.33\times10^{-6}$ m^3/Pa	$\sigma_{w_q} \approx \pm 1.4\times10^{-5}$ m^3/s	$\sigma_{w_p} \approx \pm$ 6665 Pa
Case 6	PRBS	WBS model	SNR = 21.3	SNR = 30.1
		$C_s = 2.33\times10^{-6}$ m^3/Pa	$\sigma_{w_q} \approx \pm 5.8\times10^{-6}$ m^3/s	$\sigma_{w_p} \approx \pm$ 2203 Pa

Table 2—Data for six cases to demonstrate the TS SI method. (PRBS = pseudorandom binary signal.)

Flow-rate and pressure disturbances $v_{q_{bh}}$ and $v_{p_{bh}}$ are generated as a two white-noise signals that are filtered by low-frequency Butterworth filters with cutoff frequencies $\omega \in (0 - 0.01\pi)$ rad/s. The flow-rate disturbance is considered to have more high-frequency content in accordance with what we observed in the field case discussed later in this study. Because these disturbances act as internal-excitation signals, they are filtered by the wellbore- and reservoir-system-transfer functions (Eqs. 39 and 40), and their final values are added to the noise-free bottomhole signals. Moreover, pressure and flow-rate sensor noise are simulated by adding white Gaussian noise to the bottomhole measurements. The amplitudes of the disturbances are chosen to reach predefined signal/noise ratios (SNRs). The SNR is defined as

$$SNR_{y^m} = 20\log_{10}\frac{\sigma_{y^m}}{\sigma\tilde{y}}, \quad \ldots\ldots\ldots\ldots\ldots\ldots\ldots\ldots (47)$$

where σ_{y^m} and $\sigma\tilde{y}$ are the standard deviations of the measured signal y_m and noise $\tilde{y}$, respectively.

To demonstrate the performance of the proposed two-stage (TS) system-identification (SI) method, six cases are considered. In Case 1, the single-phase wellbore model is used, whereas the other cases use the wellbore-storage (WBS) model. In these cases, the WBS effect is rather small, so to assess the robustness of the method to WBS effects, a relatively large WBS coefficient C_s is used for Cases 3 through 6. This value of C_s has a rather-substantial effect in the frequency range greater than $\omega = 10^{-4}$ rad/s. A completely variable flow-rate-wellhead signal is considered in Case 4. In Case 5, the noise level has been doubled, and in Case 6, the skin factor has been changed. In all cases, the q^m_{bh} measurement has been given a higher SNR than the p^m_{bh} measurement because in practice the uncertainty in flow-rate measurements is much higher than in pressure measurements. The specifications of different cases have been listed in **Table 2,** and the data have been plotted in **Figs. 19 through 24.** Note that only the first 10% of the data have been plotted. For all cases, the data-generating reservoir model is a homogeneous circular reservoir with a constant-pressure external boundary and properties given in Table 1.

Identification Results. Next, the synthetic signals $q_{wh}(t)$, $q^m_{bh}(t)$, and $p^m_{bh}(t)$ are used to identify discrete-time-transfer functions of the reservoir.

Results of the TS SI Method. In the first step of the TS procedure, the transfer function between q_{wh} and q^m_{bh} is identified by solving an open-loop identification problem by use of the Matlab SI toolbox (MathWorks 2015). Analyzing the periodogram of the pseudorandom binary signal for Cases 1, 2, 3, 5, and 6 shows that the amplitude of the input signal at frequencies greater than $\omega \approx 3 \times 10^{-3}$ rad/s is negligible. Therefore, we downsample the input and output data with a factor of 10. Thereafter, the output-error-

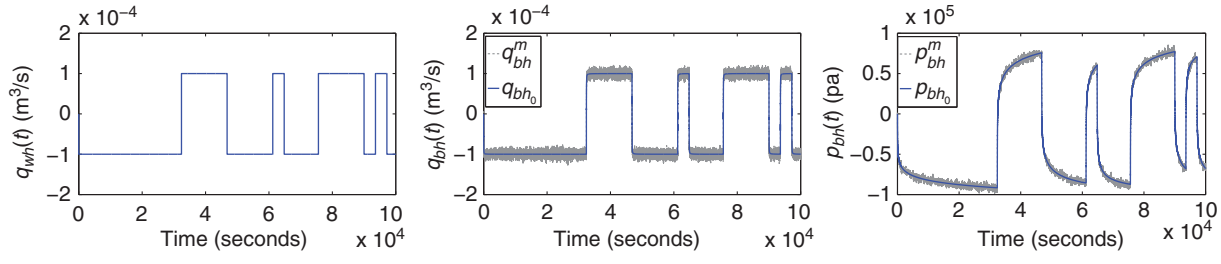

Fig. 19—Noise-free wellhead flow rate (left), and measured and noise-free bottomhole flow rates (middle) and pressures (right) for Case 1.

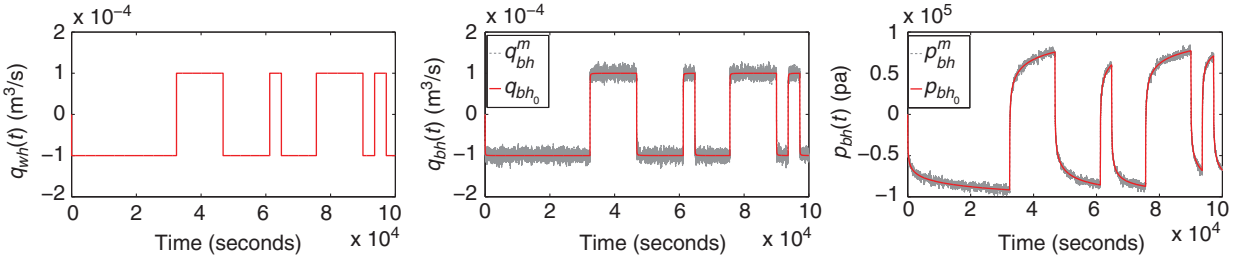

Fig. 20—Reference wellhead flow rate (left), and measured and noise-free bottomhole flow rates (middle) and pressures (right) for Case 2.

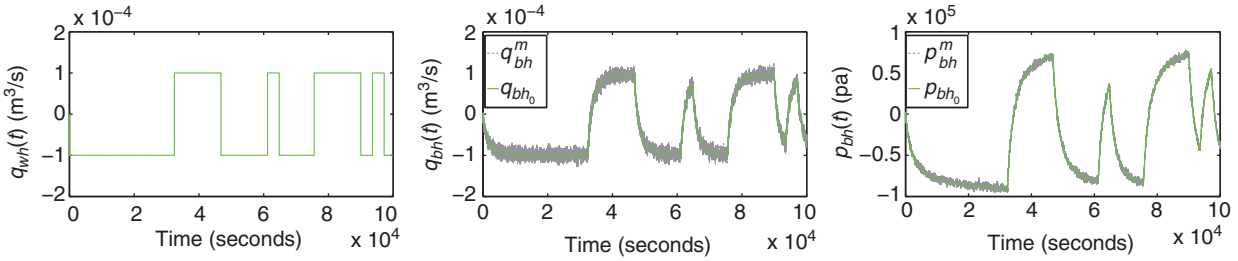

Fig. 21—Reference wellhead flow rate (left), and measured and noise-free bottomhole flow rates (middle) and pressures (right) for Case 3.

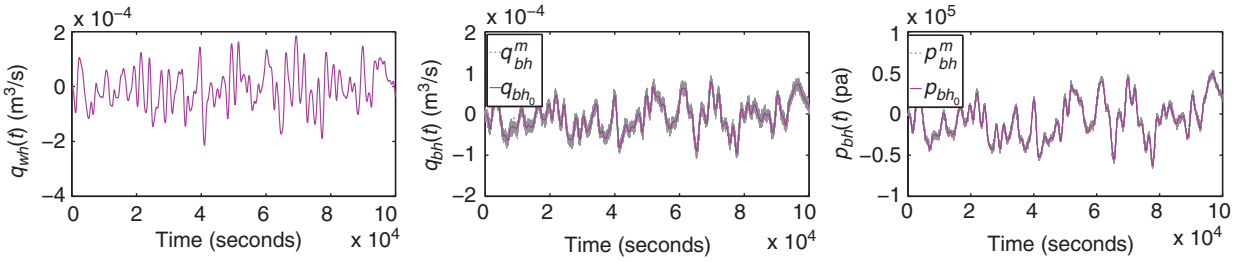

Fig. 22—Reference wellhead flow rate (left), and measured and noise-free bottomhole flow rates (middle) and pressures (right) for Case 4.

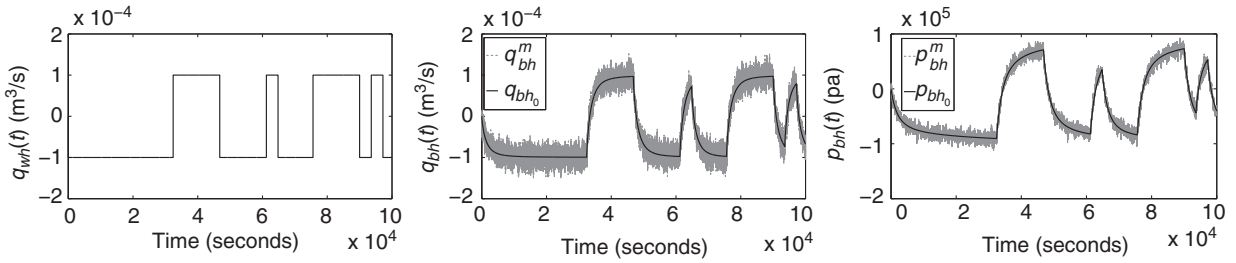

Fig. 23—Reference wellhead flow rate (left), and measured and noise-free bottomhole flow rates (middle) and pressures (right) for Case 5.

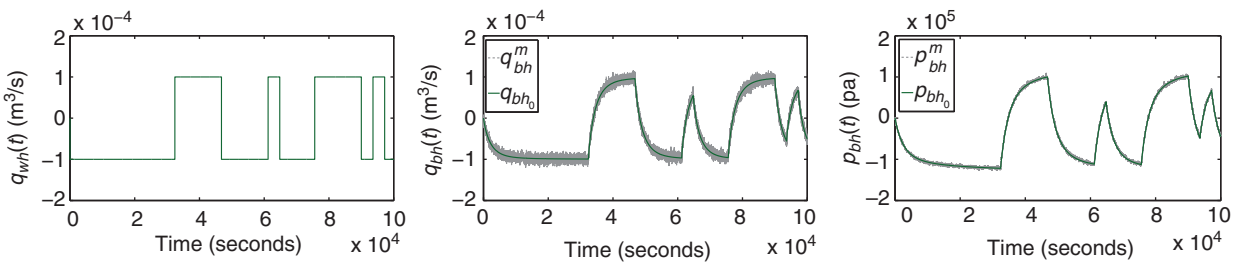

Fig. 24—Reference wellhead flow rate (left), and measured and noise-free bottomhole flow rates (middle) and pressures (right) for Case 6.

Case No.	b_0	b_1	b_2	b_3	b_4	b_5
Case 1	0.7827	0.3962	–0.6921	–0.1109	–	–
Case 2	0.7834	0.3735	–0.7026	–0.1177	–	–
Case 3	0.06395	0.01533	–0.07192	–	–	–
Case 4	0.008747	0.1707	0.01415	–0.1678	–	–
Case 5	0.06013	–0.07782	0.01925	–	–	–
Case 6	0.0234	0.02779	–0.0545	0.002316	–0.04073	0.04216
Case No.	f_1	f_2	f_3	f_4	f_5	f_6
Case 1	0.1786	–0.8024	–	–	–	–
Case 2	0.1592	–0.823	–	–	–	–
Case 3	–0.9216	–0.8749	0.8039	–0.06915)	–	–
Case 4	–0.2813	–0.4896	–0.5144	–0.4972	0.8089	–
Case 5	–2.58	2.495	–1.178	0.2636	–	–
Case 6	–1.576	0.5197	–0.8276	1.049	0.2267	–0.3911

Table 3—The estimated parameters for the first-stage identified models for the six cases.

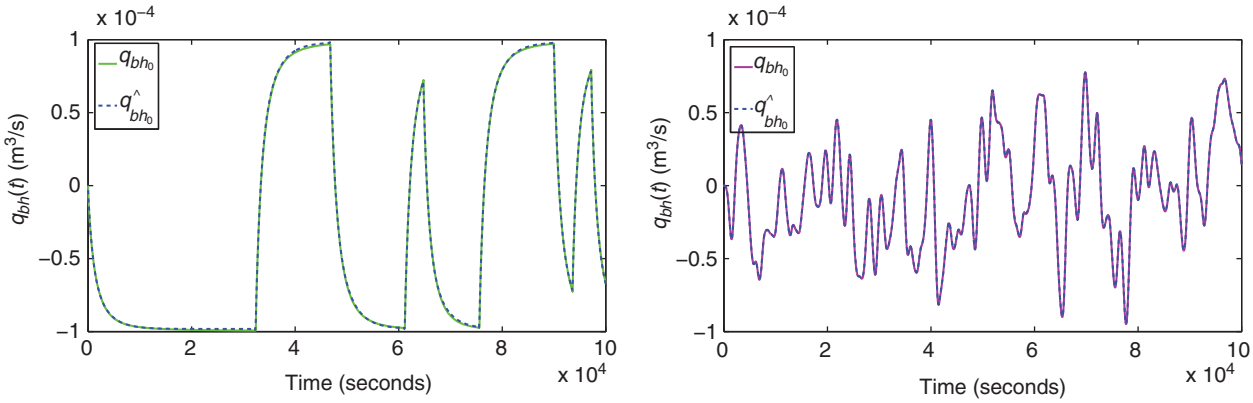

Fig. 25—Simulated $\hat{q}_{bh_0}$ by use of the first-stage identified model; (left) Case 3, (right) Case 4.

model structure is selected to estimate $G_{fs}\left(q^{-1},\hat{\theta}_N\right)$, which is an approximation of $(W_{11}S)^d$ in Eq. 39, according to

$$G_{fs}\left(q^{-1},\hat{\theta}_N\right)=\frac{\sum_{k=0}^{n_b} b_k q^{-k}}{1+\sum_{k=1}^{n_f} f_k q^{-k}}. \quad \ldots\ldots\ldots\ldots\ldots (48)$$

The parameters of the identified models—i.e., the coefficients b_k and f_k of the polynomial $\hat{\theta}_N$— have been listed in **Table 3** for the six different cases.

Before performing the second stage, or the identification of reservoir model $R_{21}^d(q^{-1})$, the transfer function $G_{fs}\left(q^{-1},\hat{\theta}_N\right)$ is used to construct $\hat{q}_{bh}(k)$ according to Eq. 43. The reconstructed bottomhole flow rates $\hat{q}_{bh}(t)$ of Cases 3 and 4 have been depicted in **Fig. 25** and show an acceptable match with the noise-free signals. Moreover, the p_{bh}^m signal is scaled down by a factor of 10^{-9} to equate the orders of magnitude of the input and output signals. In the second stage, again, the output-error structure is chosen as the model structure. The parameters of the identified models are displayed in **Table 4** for the six different cases.

Case No.	b_0	b_1	b_2	b_3	b_4	b_5
Case 1	0.3725	–0.7274	0.05723	0.5796	–0.2819	–
Case 2	0.369	–0.6789	–0.07247	0.7082	–0.3258	–
Case 3	0.3077	–0.2243	–0.4343	0.351	–	–
Case 4	0.363	–1.043	0.997	–0.3173	–	–
Case 5	0.3785	–0.7403	0.3619	–	–	–
Case 6	0.6239	–1.83	1.79	–0.5831	–	–
Case No.	b_1	b_2	b_3	b_4	b_5	b_6
Case 1	–2.307	0.8989	1.314	–1.092	0.1871	–
Case 2	–2.207	0.5235	1.835	–1.408	0.257	–
Case 3	–1.428	–0.4253	1.188	–0.3346	–	–
Case 4	–3.22	3.728	–1.795	0.2871	–	–
Case 5	–2.093	0.968	0.3628	–0.2383	–	–
Case 6	–3.241	3.764	–1.803	0.2806	–	–

Table 4—The estimated parameters for the second-stage identified models for the six cases.

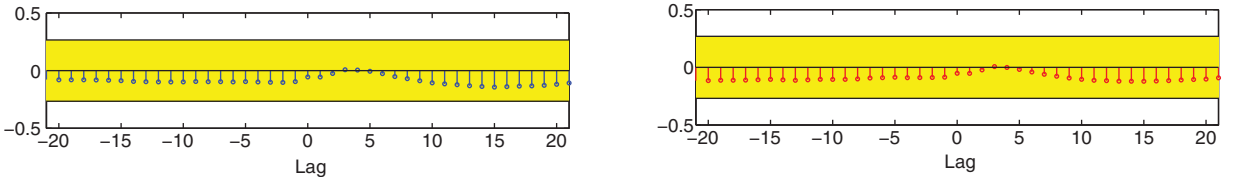

Fig. 26—CV test for the identified reservoir model in the second-stage identification; (left) Case 1, (right) Case 2.

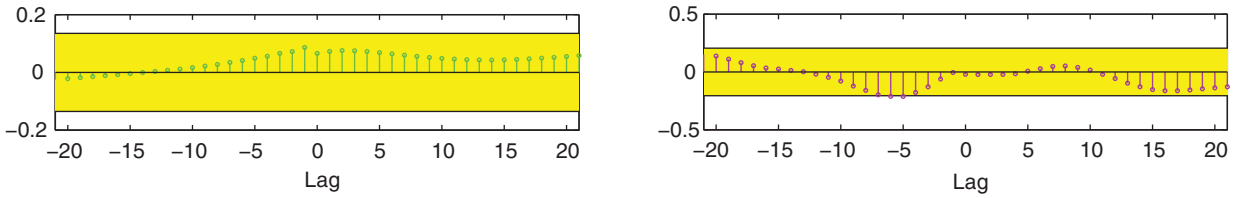

Fig. 27—CV test for the identified reservoir model in the second-stage identification; (left) Case 3, (right) Case 4.

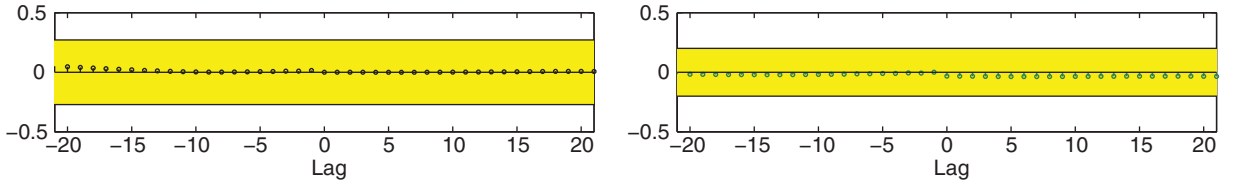

Fig. 28—CV test for the identified reservoir model in the second-stage identification; (left) Case 5, (right) Case 6.

To validate the identified models, a cross-correlation [or cross-covariance (CV)] test is performed for all the identified models in the first and second stages. The results of the CV test are presented in **Figs. 26 through 28.** In theory, a CV test is passed when the cross correlation between the identified model's prediction-error signal—ϵ in Eq. 35—and the input signal—$\bar{q}_{bh_0}$—becomes asymptotically zero. However, because of the finite length of the data, in practice a 99% confidence interval is used (the yellow area). This implies that as long as the cross-correlation signal remains within the corresponding confidence bounds, the identified model is considered to be correct with 99% confidence.

Reservoir-Type Characterization. Before use of the identified reservoir model $R_{21}^{d}\left(q^{-1},\hat{\theta}_N\right)$ for physical-parameter estimation, we have to characterize the reservoir type. In conventional pressure-transient analysis, this step is usually performed through comparing plots of the step response and its derivative with type curves of various idealized reservoir models. Following a similar reasoning, we can compare the identified model's frequency response with those of different reservoir models. In our examples it is assumed that the reservoir is homogeneous but the condition at the external boundary—e.g., infinite acting, constant pressure, or no flow—is unknown. The effect of different boundary conditions on the reservoir's frequency response has been displayed in **Fig. 29** for two different radial distances of the external boundary (1000 and 2000 m). Fig. 29 shows that a no-flow boundary causes the frequency response to raise with a high slope at low frequencies, and that a constant-pressure boundary results in a zero slope at these frequencies. However, the frequencies at which these effects can be observed are well below the frequencies for which the model has been identified. In this case, the data only contains

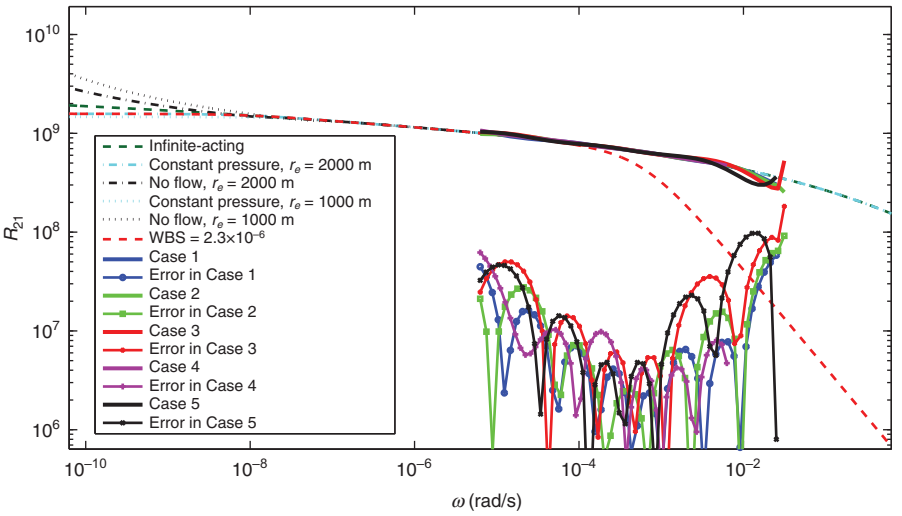

Fig. 29—Magnitude plots of the frequency responses for the identified models for Cases 1 through 5 and for the synthetic truth, displaying a small discrepancy (order of 1%).

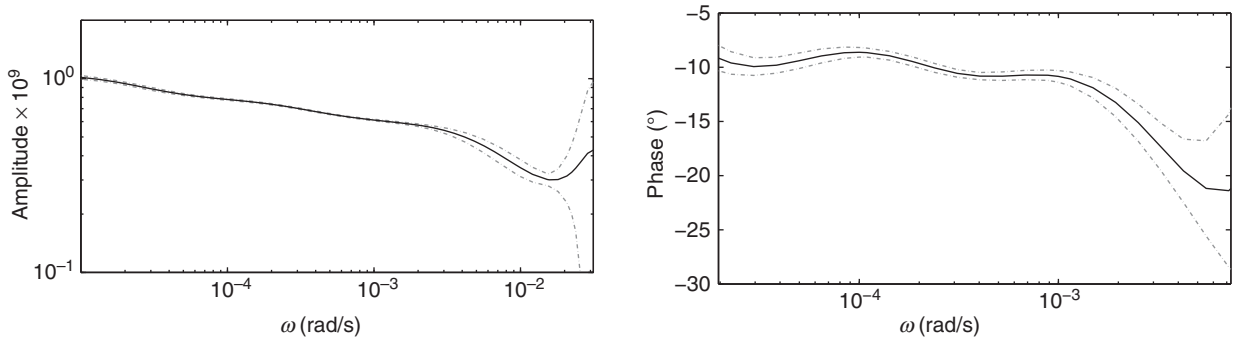

Fig. 30—The amplitude (left) and phase (right) plots of the identified model in Case 5 with the 99% confidence bounds (gray dotted lines).

Case No.	Permeability (md)	Skin	Frequency Band (rad/s)
Case 1	202.7	0.06	3×10^{-5} to 1×10^{-3}
Case 2	198.1	–0.04	3×10^{-5} to 2×10^{-3}
Case 3	200.7	0.001	3×10^{-5} to 1×10^{-3}
Case 4	194.2	–0.1	3×10^{-5} to 2×10^{-3}
Case 5	207.6	0.13	3×10^{-5} to 1×10^{-3}
Case 6	200.1	2.05	3×10^{-5} to 2×10^{-3}

Table 5—Estimated physical parameters for the six cases.

infinite-acting-reservoir information, and boundary effects are not present. Consequently, an infinite-acting-reservoir type is chosen for the physical-parameter estimation. The infinite-acting-reservoir model is obtained by letting r_e approach infinity in Eq. 25.

Physical-Parameter Estimation. According to Eq. 45, physical-parameter estimation requires the specification of a frequency range of interest (ω_L, ω_H). This range is chosen on the basis of the confidence interval of the identified model in the frequency domain. To illustrate the procedure, the frequency-response plots for Case 5 have been displayed in **Fig. 30.** These plots show that the identified reservoir model has the highest certainty at frequencies less than $\omega_H = 10^{-3}$ rad/s. The lower bound can be chosen, by use of a general rule, as four to five times the lowest measured frequency, which leads to $\omega_L = 3 \times 10^{-5}$ rad/s. The selected frequency range for each case has been listed in **Table 5.** To cover this frequency range, $M = 1{,}000$ points are selected, logarithmically distributed over the range. To put equal weight on all frequencies, the weighting function is chosen to be unity.

The parameters to be estimated are permeability k and skin factor S_r. The estimation results are listed in Table 5. In Cases 1 through 5, the "true" reservoir does not have any skin, and the estimated skin factor is almost zero. The skin factor for Case 6 is equal to 2.0, and is estimated as 2.05 (2.5% error). Also, the estimated-average-permeability values are quite close to the "true" value (200 md) with a maximum error, for Case 5, equal to approximately 3.5%.

If we compare the amplitude of the frequency response of the estimated models, by use of the estimated parameters, with that of the "truth"—i.e., the data-generating model—we find a small discrepancy (approximately less than 5%), which is outside the frequency range of interest **(Fig. 31).**

Field Example

This section describes the application of our two-stage (TS) system-identification (SI) procedure to a real-gas-well data set. The downhole transient data of a flow-after-flow (FAF) test in the gas well were obtained during a production-logging-tool (PLT) run. This FAF test was performed after the stationary passes of the PLT and covered four flow periods, each approximately 3 hours, and a short buildup of 5 hours. The total duration of the test was 65,311 seconds, where the data between 39,050 and 44,823 seconds were not recorded. For the example in this section, we select the first part of the data, until 39,050 seconds, for identification and parameter estimation, and compare the estimated results with those of a conventional pressure-transient analysis on the buildup data. At the end of the third flow period, approximately 100 recorded flow rates were clear outliers. These were removed and replaced with interpolated values. **Fig. 32 and 33** display the recorded data. The flow-rate-noise level appears to be higher than the pressure-noise level, as illustrated in the zoomed-in view in **Fig. 34.**

The surface flow-rate set points are used as the reference signal **(Fig. 35).** The downhole-pressure data are transformed to real-gas pseudopressures to linearize the governing diffusivity

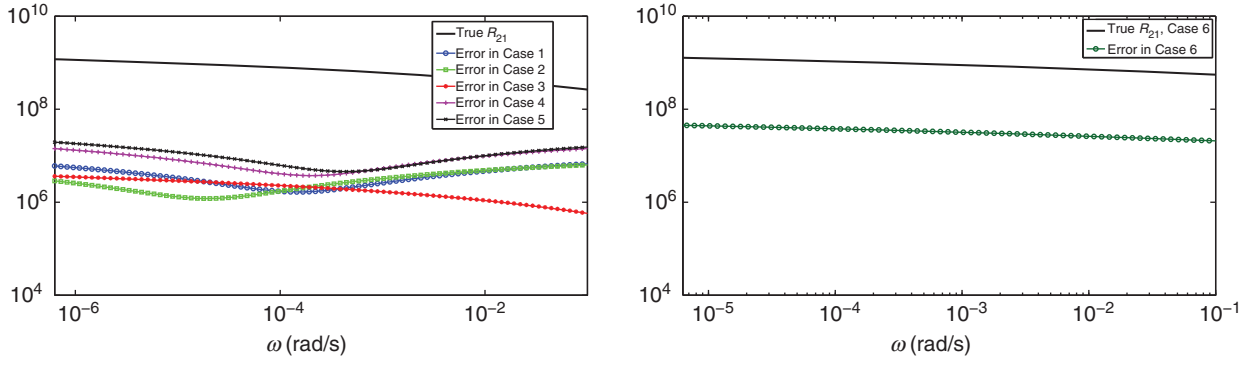

Fig. 31—Frequency-response amplitude differences between the estimated models, by use of the estimated parameters, and the data-generating model; (left) Cases 1 through 5, (right) Case 6.

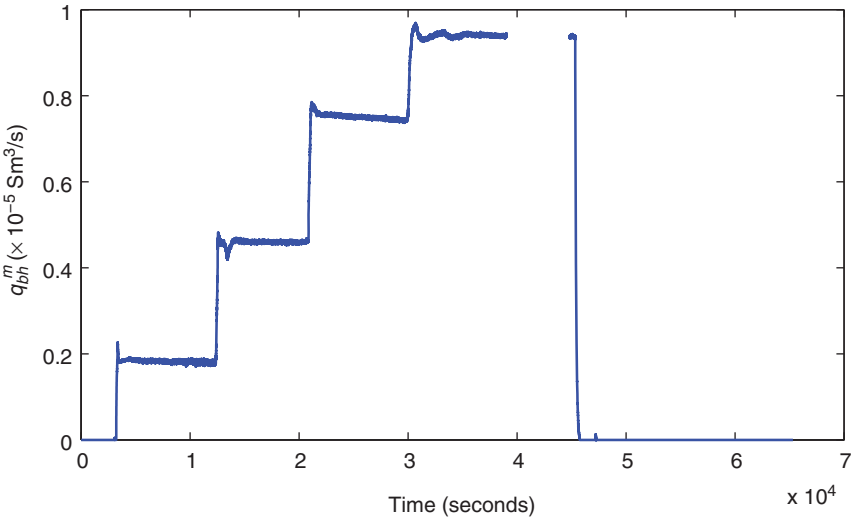

Fig. 32—Measured bottomhole flow rate in the FAF test.

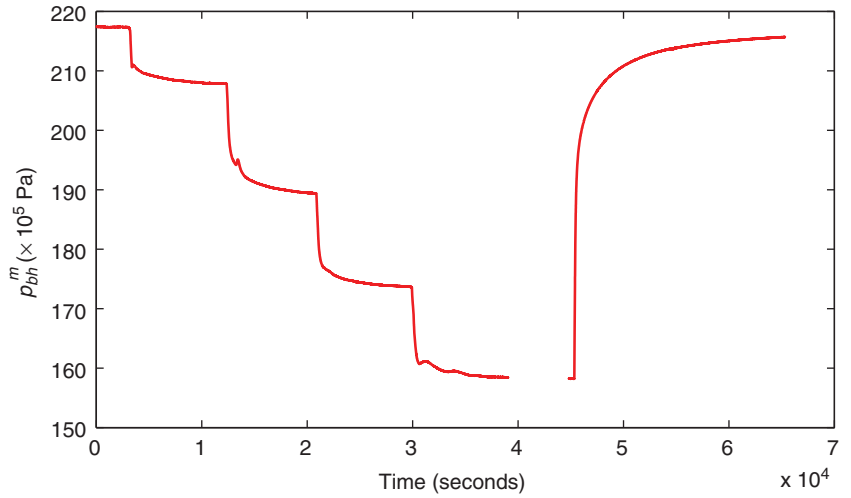

Fig. 33—Measured bottomhole pressure in the FAF test.

equation of the system (Al-Hussainy et al. 1966). In this transformation, the viscosity of the gas is estimated by use of the correlation of Carr et al. (1954). The gas specific gravity and the reservoir temperature are 0.59 and 115.5 °C, respectively. The relevant reservoir parameters are thickness = 13.1 m, porosity = 0.07, and well radius = 0.0762 m.

The identification in the first step yields an eighth-order Box-Jenkins (BJ) model (Box et al. 1994) for $G_{fs}\left(\hat{\theta}, q^{-1}\right)$, which describes the dynamic relationship between the reference and the measured downhole flow-rate signal. The identification in the second step estimates a sixth-order output-error model for $G_{ss}\left(\hat{\theta}, q^{-1}\right)$. To perform the second step, the output is scaled down with a factor of 10^{-18} to make its order of magnitude the same as that of the input. The frequency response of the identified reservoir model in the second-stage is displayed in **Fig. 36.** We use the confidence bounds of $G_{ss}\left(\hat{\theta}, q^{-1}\right)$ to select the frequency range $(\omega_L - \omega_H)$ for physical-parameter estimation, because

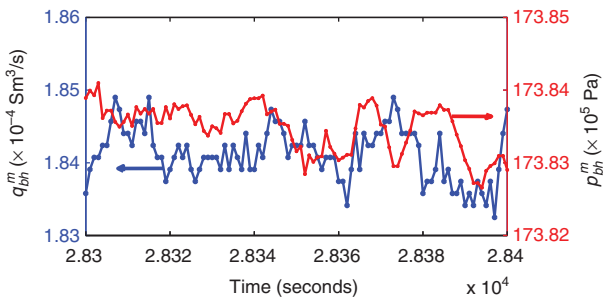

Fig. 34—Zoomed-in view of the bottomhole flow rate and pressure signals, illustrating the difference in noise level; (left axis) flow rate, (right axis) pressure.

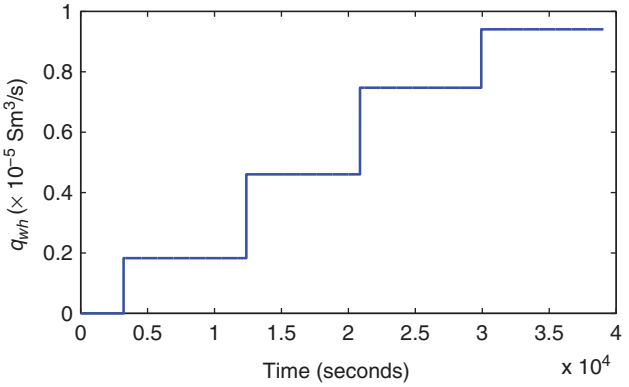

Fig. 35—Wellhead flow-rate set-point signal used as reference flow-rate signal.

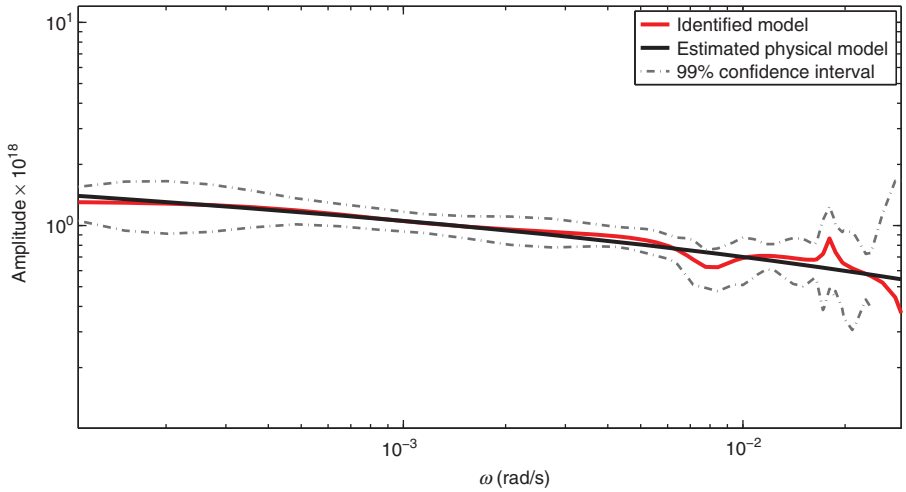

Fig. 36—Magnitude plots of the identified model from TS SI and of the physics-based model by use of the estimated physical parameters.

spectral analysis of the q_{bh} signal does not show a clear ω_H cutoff. The confidence interval of $G_{ss}\left(\hat{\theta}, q^{-1}\right)$ (gray dotted lines in Fig. 36) indicates that the model is less reliable at frequencies greater than $\omega = 10^{-2}$ rad/s because the interval starts to grow in this range. On the other hand, the number of data points determines the lowest-frequency resolution to be 10^{-4} rad/s. Hence, a frequency range $\omega = \left(4 \times 10^{-4} - 10^{-2}\right)$ rad/s is selected. Although this constitutes a relatively narrow frequency band for the physical-parameter estimation, it turns out to be wide enough to produce acceptable results.

There is no evidence of a constant-pressure or no-flow boundary—i.e., a horizontal line or an upward straight line—in the selected frequency range; therefore, a parameterized infinite-acting gas-reservoir model is selected for physical-parameter estimation. There is also no indication for wellbore storage, which would result in a sharp drop in amplitude at higher frequencies (dashed red line in Fig. 29). The parameterized physical model of an infinite-acting gas reservoir in pseudopressure—i.e., $G_{\text{inf}}(k, S_t)$—is used for parameter estimation; Appendix D provides the derivation of G_{inf}. Conducting the parameter-estimation optimization according to Eq. 45, by use of the identified model and the parameterized physical model, results in estimated permeability and total skin values of 10.3 md and −2.4, respectively. These estimated values are consistent with the estimates for permeability and skin obtained from the final buildup, by use of a straight-line analysis, which are 10.9 md and −2.6, respectively. As a comparison we also performed a classic deconvolution analysis with the aid of commercial well-testing software, which is described in Appendix E. Although the resulting parameter values are in the same range as the values estimated with the aid of SI, it is clear that the (somewhat arbitrary) choice of the constant-rate approximation of the flow rates and the weight factors, as required in the total-least-square-based deconvolution procedure implemented in this software, can have a significant influence on the shape of the computed impulse response and the estimated parameters.

Conclusions

The conclusions of this study are as follows:

1. Pressure-transient analysis (PTA) can be interpreted as a form of system identification (SI); i.e., as a process to identify a mathematical model from noisy data. Modern SI techniques, as applied in advanced process engineering, can also be used in PTA, and could be of particular value for the estimation of reservoir parameters by use of continuous bottomhole-pressure and flow-rate measurements.
2. Single-phase near-compressible flow in a circular reservoir can be described in the Laplace domain with the aid of four transfer functions relating pressures and flow rates at the sandface of the well and the external reservoir boundary. A similar set of transfer functions can be obtained to describe the flow in a well, relating pressures and flow rates at surface and downhole. Alternatively, a Laplace-domain representation of a well with wellbore storage can be derived in terms of two transfer functions, relating only the flow rate at surface to the downhole variables.
3. Coupling of the sets of reservoir- and wellbore-transfer functions reveals the causal structure of the combined reservoir/wellbore system. In particular, the wellbore acts as a feedback mechanism that intrinsically couples fluctuations in bottomhole pressure and flow rates. This implies that it will not be possible to identify a reservoir model—i.e., the relevant reservoir-transfer function—by use of only information from noisy downhole data.
4. The use of an auxiliary measurement, taken outside the feedback loop, will restore the identifiability of the reservoir model. In this study we used the surface flow rate as an auxiliary signal, but other choices, not detailed here, may be possible. Moreover, underlying assumptions for identifiability in our paper are a nearly linear relationship between downhole pressures and flow rates, and a nearly noise-free auxiliary signal. Relaxing these assumptions may be possible, but has not been addressed in our study.
5. The presence of a feedback loop in the combined reservoir/wellbore system leads to the requirement to use closed-loop SI techniques. In particular, a two-stage (TS) SI method has been used in this study to estimate a discrete-time-domain reservoir model. In the first stage, the effects of process noise and sensor noise are removed from the data, and an estimate of a noise-free bottomhole flow rate is obtained. In the second stage, this flow-rate signal is then used to identify the reservoir model.
6. To obtain estimates of physical reservoir parameters (e.g., average permeability and skin factor), it is necessary to compare the response of the identified reservoir model to those of known reservoir models with typical geometries and boundary conditions. By use of classic PTA theory, the latter are conveniently obtained in the Laplace domain, whereas the identified model is in the time domain. The comparison, using an optimization approach to minimize the mismatch between measured and modeled data, can be performed in the frequency domain by transferring the identified and known reservoir models from their time and Laplace domains, respectively.
7. An important advantage of our proposed TS SI method is that it can directly operate on the recorded flow-rate signal as measured and does not require the availability of a piecewise-constant flow-rate signal, unlike existing PTA methods that use time-domain deconvolution. Accordingly, breakpoint detection

is not required and arbitrarily fluctuating downhole-pressure and flow-rate signals can be used for the identification. In addition, this feature offers the opportunity to design deliberate flow-rate disturbances at surface—e.g., in the form of periodic or random fluctuations in surface flow rate or choke settings on top of a steady-state signal—to maximize the information content in the downhole signals.

8. The results of six numerical experiments by use of a synthetic data set, and of a field case by use of real data from a gas well, illustrate the potential of the TS SI method to estimate reservoir parameters from noisy downhole-pressure and flow-rate data. In the experiments that use synthetic data, we estimated the average permeability and skin of a reservoir on the basis of downhole signals with various noise levels, and obtained estimates within a few percent of the true values. In the experiment with real downhole data of a gas well, we obtained permeability and skin values that closely match those obtained from a traditional buildup analysis and a conventional deconvolution procedure.
9. The application of SI approaches from the process-engineering community to PTA of downhole-pressure and flow-rate data leads to novel theoretical insights (in particular, the interpretation of wellbore storage as an internal-feedback mechanism), and potentially useful applications (in particular, methods to cope with correlated pressure and flow-rate noise, and without the need for piecewise-constant flow rates). However, further testing of the proposed methods on real data will be required to fully assess this potential.

Nomenclature

a = velocity of water-hammer wave in the fluid, m/s
A = cross-sectional area of the pipe, m^2
C_s = wellbore-storage coefficient, m^3/Pa
C_t = total compressibility, 1/Pa
D = internal diameter of the pipe, m
e = wall thickness of the pipe, m
E = Young's modulus of the pipe, Pa
g = acceleration of gravity, m/s^2
G = system model-transfer function
h = reservoir thickness, m
H = noise model-transfer function, or hydraulic head, m
$I_\#$ = modified Bessel's function of the first kind
j = imaginary unit
k = discrete time, or absolute permeability, m^2
K = bulk modulus of the fluid, Pa
$K_\#$ = modified Bessel's function of the second kind
p = pressure, Pa
q = shift operator, or flow rate, m^3/s
r = radial distance, m
R = laminar flow friction, 1/s
s = Laplace variable
S_r = skin factor
T = time, seconds
v = process noise
$\tilde{v}$ = sensor noise
z = z-domain variable, or vertical distance, m
β = physical parameter vector
η = hydraulic diffusivity, 1/s
θ = model parameter vector
μ = fluid viscosity, Pa·s
ν = kinematic fluid viscosity, m^2/s
ρ = fluid density, kg/m^3
σ = standard deviation
ϕ = porosity
ω = angular frequency, rad/s

Subscript

bh = bottomhole
r = reservoir
w = wellbore
wh = well head

Superscript

d = discrete time
m = measured
0 = true

Acknowledgments

The authors acknowledge the late Farhad Ali Farhadpour of Sharif University of Technology for introducing them to this problem; Arne Dankers from Delft University of Technology for valuable discussions; Dana Energy Company of Iran for providing a part of the financial support of the research; and Kappa Petroleum E&P Software for providing an academic Saphir license.

References

Ahn, S. and Horne, R. 2011. The Use of Attenuation and Phase Shift to Estimate Permeability Distributions from Pulse Tests. Presented at the SPE Annual Technical Conference and Exhibition, Florence, Italy, 19–22 September. SPE-146636-MS. http://dx.doi.org/10.2118/146636-MS.

Al-Hussainy, R., Ramey, H. Jr., Crawford, P., et al. 1966. The Flow of Real Gases Through Porous Media. *J Pet Technol* **18** (5): 624–636. SPE-1243-A-PA. http://dx.doi.org/10.2118/1243-A-PA.

Athichanagorn, S. 1999. *Development of an Interpretation Methodology for Long-Term Pressure Data from Permanent Downhole Gauges*. PhD dissertation, Stanford University, Stanford, California (June 1999).

Baygü, B., Kuchuk, F. and Arikan, O. 1997. Deconvolution Under Normalized Autocorrelation Constraints. *SPE J.* **2** (3): 246–253. SPE-28405-PA. http://dx.doi.org/10.2118/28405-PA.

Bosgra, O. 2010. *Physical Modelling for Systems and Control*. Delft University of Technology. http://www.pvandenhof.nl/Reportfiles/Bosgra2010.pdf

Bourgeois, M. and Horne, R. N. 1993. Well Test Model Recognition Using LaPlace Space Type Curves. *SPE Form Eval* **8** (1): 17–25. SPE-22682-PA. http://dx.doi.org/10.2118/22682-PA.

Box, G. E. P., Jenkins, G. M. and Reinsel, G. C. 1994. *Times Series Analysis: Forecasting and Control,* third edition. Englewood Cliffs: Prentice Hall.

Carr, N. L., Kobayashi, R., and Burrows, D. B. 1954. Viscosity of Hydrocarbon Gases Under Pressure. *J Pet Technol* **6** (10): 47–55. SPE-297-G. http://dx.doi.org/10.2118/297-G.

Chaudhry, M. H. 1979. *Applied Hydraulic Transients*. New York City: Van Nostrand Reinhold Inc.

Cheng, Y., Lee, W. J. and McVay, D. A. 2005. Application of Fast Fourier Transforms to Deconvolution of Multirate Well-Test Data. Presented at the SPE Annual Technical Conference and Exhibition, Dallas, 9–12 October. SPE-96032-MS. http://dx.doi.org/10.2118/96032-MS.

Forssell, U. and Ljung, L. 1999. Closed-Loop Identification Revisited. *Automatica* **35** (7): 1215–1241. http://dx.doi.org/10.1016/S0005-1098(99)00022-9.

Gringarten, A. 2008. From Straight Lines to Deconvolution: The Evolution of the State of the Art in Well Test Analysis. *SPE Res Eval & Eng* **11** (1): 41–62. SPE-102079-PA. http://dx.doi.org/10.2118/102079-PA.

Gustavsen, B. and Semlyen, A. 1999. Rational Approximation of Frequency Domain Responses by Vector Fitting. *IEEE Trans. Power Deliver.* **14** (3): 1052–1061. http://dx.doi.org/10.1109/61.772353.

Hassanzadeh, H. and Pooladi-Darvish, M. 2007. Comparison of Different Numerical Laplace Inversion Methods for Engineering Applications. *Appl. Math. Comput.* **189** (2): 1966–1981. http://dx.doi.org/10.1016/j.amc.2006.12.072.

Kamal, M. M. and Abbaszadeh, M. 2009. *Transient Well Testing*. Richardson, Texas: Monograph Series, Society of Petroleum Engineers.

Kappa Saphir (Ecrin package, evaluation version). 2015. http://www.kappaeng.com/software/saphir. Accessed 2 April 2015.

Kuchuk, F. 1990. Applications of Convolution and Deconvolution to Transient Well Tests. *SPE Form Eval* **5** (4): 375–384. SPE-16394-PA. http://dx.doi.org/10.2118/16394-PA.

Kuchuk, F. J., Onur, M. and Hollaender, F. 2010. *Pressure Transient Formation and Well Testing: Convolution, Deconvolution and Nonlinear Estimation*, Vol. 57. Amsterdam: Elsevier Science.

Kuiper, I. T. J. 2009. *Well Testing in the Framework of System Identification–An Exploratory Study*. Master's thesis, Delft University of Technology, the Netherlands (February 2009).

Levitan, M. 2005. Practical Application of Pressure-Rate Deconvolution to Analysis of Real Well Tests. *SPE Res Eval & Eng* **8** (2): 113–121. SPE-84290-PA. http://dx.doi.org/10.2118/84290-PA.

Ljung, L. 1999. *System Identification: Theory for the User*. Upper Saddle River, New Jersey: Prentice Hall.

Mansoori, M., Dankers, A. and Van den Hof, P. 2014. Errors-in-Variables Identification in Bilaterally Coupled Systems with Application to Oil Well Testing. Proc., 19th IFAC World Congress, Cape Town, South Africa, 24–29 August, Vol. 1, 4656–4661. http://dx.doi.org/10.3182/20140824-6-ZA-1003.01491.

Mansoori, M., Dankers, A., Van den Hof, P., et al. *In press*. Underground Reservoir Identification using Generalized Wellbore Data. 17th IFAC Symposium on System Identification, 19–21 October, Beijing, China (submitted February 15, 2015).

MathWorks. 2015. System Identification Toolbox. http://www.mathworks.com/products/sysid/

Nomura, M. and Horne, R. N. 2009. Data Processing and Interpretation of Well Test Data as a Nonparametric Regression Problem. Presented at the SPE Western Regional Meeting, San Jose, California, 24–26 March. SPE-120511-MS. http://dx.doi.org/10.2118/120511-MS.

Onur, M. and Reynolds, A. 1998. Well Testing Applications of Numerical Laplace Transformation of Sampled-Data. *SPE Res Eval & Eng* **1** (3): 268–277. SPE-36554-PA. http://dx.doi.org/10.2118/36554-PA.

Oppenheim, A. V., Schafer, R. W. and Buck, J. R. 1999. *Discrete-Time Signal Processing*, Vol. **5**. Upper Saddle River, New Jersey: Prentice Hall.

Pimonov, E., Ayan, C., Onur, M., et al. 2010. A New Pressure/Rate-Deconvolution Algorithm To Analyze Wireline Formation-Tester and Well-Test Data. *SPE Res Eval & Eng* **13** (4): 603–613. SPE-123982-PA. http://dx.doi.org/10.2118/123982-PA.

Press, W. H., Teukolsky, S. A., Vetterling, W. T., et al. 2007. *Numerical Recipes: The Art of Scientific Computing*, third edition, Section 5.12 Padé Approximants. Cambridge: Cambridge University Press.

Roumboutsos, A. and Stewart, G. 1988. A Direct Deconvolution or Convolution Algorithm for Well Test Analysis. Presented at SPE Annual Technical Conference and Exhibition, Houston, 2–5 October. SPE-18157-MS. http://dx.doi.org/10.2118/18157-MS.

Söderström, T. 2007. Errors-in-Variables Methods in System Identification. *Automatica* **43** (6): 939–958. http://dx.doi.org/10.1016/j.automatica.2006.11.025.

Söderström, T., Wang, L., Pintelon, R., et al. 2013. Can Errors-in-Variables Systems be Identified from Closed-Loop Experiments? *Automatica* **49** (2): 681–684, http://dx.doi.org/10.1016/j.automatica.2012.11.017.

Stehfest, H. 1970. Algorithm 368: Numerical Inversion of Laplace Transforms. *Comm. ACM* **13** (1): 47–49. http://dx.doi.org/10.1145/361953.361969.

Van den Hof, P. M. J. 1998. Closed-Loop Issues in System Identification. *Annu. Rev. Control* **22:** 173–186. http://dx.doi.org/10.1016/S1367-5788(98)00016-9.

Van den Hof, P. M. J. and Schrama, R. J. 1993. An Indirect Method for Transfer Function Estimation from Closed Loop Data. *Automatica* **29** (6): 1523–1527. http://dx.doi.org/10.1016/0005-1098(93)90015-L.

von Schroeter, T., Hollaender, F. and Gringarten, A. C. 2004. Deconvolution of Well-Test Data as a Nonlinear Total Least-Squares Problem. *SPE J.* **9** (4): 375–390. SPE-77688-PA. http://dx.doi.org/10.2118/77688-PA.

Appendix A—System Identification

A physical process is linear-time invariant (LTI) if it displays linear dynamic behavior and its properties do not change with time. Mathematically, an LTI system can be described by linear ordinary-differential (or partial-differential) equations with time-independent coefficients. The response or the output $y(t)$ of the LTI system, to an input $u(t)$, can be described by a convolution integral as

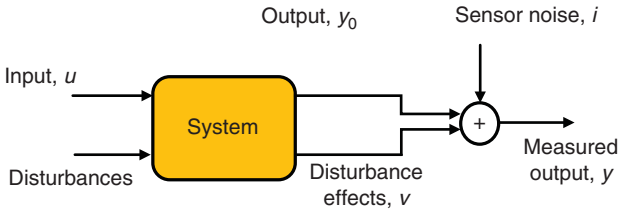

Fig. A-1—Block-diagram representation of a dynamical system under the effects of input, disturbances, and sensor noise.

$$y(t) = \int_0^t u(\tau) \cdot g(t-\tau)\ \mathrm{d}\tau = \int_0^t \frac{\mathrm{d}\,u(\tau)}{\mathrm{d}t} \cdot k(t-\tau)\mathrm{d}\tau, \quad \ldots\ldots\ldots\ldots\ldots\ldots\ldots\ldots (A\text{-}1)$$

in which $g(t) = \dfrac{\mathrm{d}\,k(t)}{\mathrm{d}t}$ and $k(t)$ are the impulse and step responses of the system, respectively. This property is also known as Duhamel's principle. In the Laplace domain, Eq. A-1 is written as [taking into account that $u(0) = k(0) = 0$]

$$\mathcal{Y}(s) = G(s)\mathcal{U}(s) = sK(s)\mathcal{U}(s), \quad \ldots\ldots\ldots\ldots\ldots\ldots (A\text{-}2)$$

where s is the Laplace variable, $\mathcal{U}(s)$ and $\mathcal{Y}(s)$ are the Laplace transforms of $u(t)$ and $y(t)$, and $G(s)$ and $K(s)$ are the Laplace transforms of the impulse and step responses. $G(s)$ is also called the transfer function of the system. Theoretically, the impulse response, step response, or transfer function can entirely characterize the dynamic behavior of the LTI system. Hence, in many applications the impulse response or the transfer function of the physical system has to be obtained for further investigation of the dynamical behavior of the system. For example, in classical pressure-transient analysis, a reservoir-flow model is identified by analyzing the step response of a reservoir and its derivative with respect to the natural logarithm of time; the latter is simply the impulse-response function multiplied by time:

$$\frac{\mathrm{d}\,k(t)}{\mathrm{d}(\ln t)} = tg(t). \quad \ldots\ldots\ldots\ldots\ldots\ldots\ldots\ldots (A\text{-}3)$$

To obtain the impulse response, one can write all the governing equations of the physical processes and solve the set of equations for an impulse-boundary condition. This approach is called first-principle or white-box modeling and leads to a physically insightful model of the system. However, deriving such a model for a complex system is usually difficult, if possible at all. An alternative approach that is widely used to model complex systems is data-driven or black-box modeling, which results in a mathematical model for the system derived from known-input and measured-output data. In reality, the system is affected by unknown disturbances in addition to the input, the influences of which are also present in the observed output; these effects are called process noise and denoted by v throughout the study. Moreover, when a sensor is used to measure the observed output, measurement errors, also called sensor noise and denoted by $\tilde{v}$, corrupt the measured values. Thus, what is measured as the output of the system is the summation of the input effect, the disturbances, and the sensor noise. In **Fig. A-1,** the system, input, output, disturbances, and sensor noise are shown in a block-diagram representation to show the causal relationship of the system and its environment. System identification (SI) techniques are data-driven methods for modeling dynamical systems that rigorously deal with the statistical effects of the sensor noise and disturbances in the data and can be implemented in different noise- and data-availability situations. The obtained mathematical model

does not directly allow for a physical interpretation and just represents a relationship between the input and output data. This identified model can be used to predict or simulate the response of the system to different inputs; therefore, calculating this model implicitly means the calculation of the impulse, or step response, of the system.

Because measurement devices typically record values at discrete-time intervals, the recorded input and output are $y(kT)$ and $u(kT)$, $k=0, 1, 2, \ldots$, where T is the sampling period. Thus, the relationship between the sampled input and output can be expressed in discrete time as

$$y(k) = G^0(q)u(k) + w(k), \quad k = 0, 1, \ldots, N, \quad \ldots\ldots\ldots \quad \text{(A-4)}$$

where G^0 is a discrete-time-transfer function and q^{-1} is the shift operator; i.e., $q^{-1}u(k) = u(k-1)$. The variable $w(k)$ represents a combination of sensor and process noise and can be modeled as a stochastic signal. The process noise and sometimes also the sensor noise are caused by an unknown physical phenomenon, which is normally not instantaneous such that its effects linger on. Hence, the value of the stochastic signal at a certain time is correlated with its values at the previous times. This property is called autocorrelation and implies that it is not reasonable to model the stochastic signal as white noise. (White noise is a signal with samples that are regarded as a sequence of serially uncorrelated random variables with zero mean and finite variance.) Consequently, the noise signal should be modeled as a filtered white noise $w(k) = H^0(q)e(k)$, where H^0 is a monic, stable, minimum-phase filter, and e is white noise. If there is no high-frequency content in the measured signals greater than half the sampling frequency (called the Nyquist frequency), then there is a direct relationship between G^0 in Eq. A-4 and G in Eq. A-2. In particular, both transfer functions have the same frequency response in the frequency range $\omega \in (-\omega_s/2, \omega_s/2)$ where ω_s is the sampling frequency. To ensure that there is no high-frequency content in the measured signals, either antialiasing filters can be used to take the measurements or the sampling rate can be increased. The main point is that if an estimate of the discrete-time-transfer function G^0 in Eq. A-4 is obtained by use of tools from SI, the continuous-time dynamics of the physical system can be inferred from this estimate.

To analyze properties of the estimated transfer functions obtained by use of SI methods, it is convenient to suppose that the data set was generated by Eq. A-4. Then, the goal of SI can be stated as obtaining estimates of the transfer function G^0 (and sometimes, but not always, H^0) of the data-generating system in Eq. A-4 on the basis of the measured data $[u(k), y(k)]_{k=1,\cdots,N}$.

A powerful SI method is the prediction-error method (PEM). The main philosophy of the prediction-error framework is to find a model from a set of candidate models that can predict the current value of an output of a system given the input to the system and past values of the output. This optimal model is selected in such a way that has the best predictive capabilities; more information is provided in Appendix B. Note that the selected model set does not have any physical meaning and simply represents a regression between the input and past values of the system.

To obtain an estimate of the transfer functions G^0 and H^0, a set of candidate models needs to be defined. One way is to use parameterized transfer functions. There are several black-box-model sets that can be selected for fitting the data and estimating the system and noise models. For example, in the Box-Jenkins model (Box et al. 1994) structure, the system and noise models are independently parameterized as $G(q^{-1}, \theta) = B(q^{-1}, \theta)/F(q^{-1}, \theta)$ and $H(q^{-1}, \theta) = C(q^{-1}, \theta)/D(q^{-1}, \theta)$, where B, C, D, and F are polynomials in the shift operator q^{-1}:

$$G(q, \theta) = \frac{b_0 + b_1 q^{-1} + \cdots + b_{n_b} q^{-n_b}}{1 + f_1 q^{-1} + \cdots + f_{n_f} q^{-n_f}} \text{ and}$$

$$H(q, \theta) = \frac{1 + c_1 q^{-1} + \cdots + c_{n_c} q^{-n_c}}{1 + d_1 q^{-1} + \cdots + d_{n_d} q^{-n_d}}, \quad \ldots\ldots\ldots\ldots \quad \text{(A-5)}$$

where the parameter vector $\theta = [b_0 \cdots b_{n_b} f_1 \cdots f_{n_d} c_1 \cdots c_{n_c} d_1 \cdots d_{n_d}]^T$ is the vector of unknown parameters that need to be determined. Note that the noise model $H(q)$ is monic; i.e., if hypothetically q^{-1} is substituted with zero, $H = 1$. For the simpler autoregressive-external-input-model structure, $C = I$ and $D = F$, and for the output-error-model structure, $H = I$. Typically θ is restricted to any vector that results in stable $G(q,\theta)$ and stable, minimum phase $H(q,\theta)$. These model sets do not have physical meaning and just represent the correlation in the data.

In the prediction-error framework, it can be shown that such a predictor model has the form (Appendix B)

$$\hat{y}(k|k-1, \theta) = H^{-1}(q, \theta)G(q, \theta)u(k) + [1 - H^{-1}(q, \theta)]y(k), \quad \ldots\ldots\ldots\ldots\ldots\ldots \quad \text{(A-6)}$$

where $\hat{y}(k|k-1, \theta)$ denotes the prediction of y at time k given the input u for all time up to time k and the output y for all time up to time k–1. The last step in SI is to define a selection rule that is used to select the best model out of the set of candidate models. As the name suggests, prediction-error methods are dependent on selecting models that make the best predictions (i.e., have the smallest prediction errors):

$$\hat{\theta}_N = \underset{\theta}{\operatorname{argmin}} \frac{1}{N} \sum_{k=1}^{N} \varepsilon^2(k, \theta), \quad \ldots\ldots\ldots\ldots\ldots\ldots \quad \text{(A-7)}$$

in which ε is the prediction error:

$$\varepsilon(k, \theta) = y(k) - \hat{y}(t|t-1, \theta) = H^{-1}(q, \theta)[y(k) - G(q, \theta)u(k)]. \quad \ldots\ldots\ldots\ldots\ldots\ldots \quad \text{(A-8)}$$

The parameter vector $\hat{\theta}$ is usually obtained by performing a nonlinear optimization. The noise in the measurements causes the estimated parameter vector to be a random variable with normal distribution:

$$\hat{\theta} \in \mathcal{N}(\theta_0, P_{\hat{\theta}}), \quad \ldots\ldots\ldots\ldots\ldots\ldots\ldots\ldots \quad \text{(A-9)}$$

where $P_{\hat{\theta}}$ is the estimated covariance matrix and θ_0 is the true parameter vector. An important property of the covariance matrix is that it asymptotically approaches zero as the number of measurements approaches infinity; i.e., for experiments with an infinite number of measurements, $\hat{\theta}$ approaches θ_0 and SI leads to an unbiased estimate of the system. To validate the identified model, different statistics-based tests such as residual tests can be carried out. For example, by use of $P_{\hat{\theta}}$, the cross-correlation test that will be used in this study is such that one can conclude with 99% confidence that there is no evidence in the data that the estimated model is wrong.

The benefits of using PEM for modeling complex systems include rigorous handling of the process and sensor noise, whether white or colored; effectively working on the recorded digital signal without requiring a piecewise-constant approximation of the signals; providing the statistical properties of the identified model; and leading to a parametric model that can be used for prediction, simulation, or control purposes.

Appendix B—Prediction-Error Framework for System Identification (SI)

A powerful SI method is the prediction-error method (Ljung 1999). Consider the following informal presentation of a predictor model that forms the basis of the prediction-error framework (Ljung 1999). Suppose that we want to predict y in Eq. A-4 at time k given $u(k)$ and $y(k)$, $k=0, 1, 2, \ldots, n-1$ (i.e., all past values of the input and output are known). In addition, suppose that both G^0 and H^0 are known; recall that $v(k) = H^0(q)e(k)$, where e is white noise. Because H^0 is monic, the output can be expressed as

$$\begin{aligned} y(k) &= G^0(q)u(k) + H^0(q)e(k) \\ &= G^0(q)u(k) + [H^0(q) - 1]e(k) + e(k) \\ &= G^0(q)u(k) + [H^0(q) - 1]H^{0^{-1}}(q)v(k) + e(k) \\ &= G^0(q)u(k) + [1 - H^{0^{-1}}(q)]v(k) + e(k) \end{aligned} \quad \ldots \quad \text{(B-1)}$$

The first term is known because it consists of the known transfer function G^0 and the known input. The second term of Eq. B-1 consists of only past values of the noise, and thus is also known. To see why, consider expressing $v(k)$ as

$$v(k) = y(k) - G^0(q)u(k). \quad \ldots \quad \text{(B-2)}$$

Because $y(k)$ and $u(k)$ are known for $k = 0, 1, \ldots, n-1$, it follows from Eq. B-2 that $v(k)$ is also known for $k = 0, 1, \ldots, n-1$. Last, the third term in Eq. B-1 is not knowable, because $e(k)$ is an independent random variable. We do know, however, that the expected value of $e(k)$ is zero. Thus, the expected value of the output y, given the input and past output, is

$$\hat{y}(k|k-1) = G^0(q)u(k) + [1 - H^{0^{-1}}(q)]v(k). \quad \ldots \quad \text{(B-3)}$$

Substituting the expression for v in terms of u and y (Eq. B-2), into Eq. B-3 results in

$$\begin{aligned} \hat{y}(k|k-1) &= G^0(q)u(k) + [1 - H^{0^{-1}}(q)][y(k) - G^0(q)u(k)] \\ &= H^{0^{-1}}(q)G^0(q)u(k) + [1 - H^{0^{-1}}(q)]y(k), \end{aligned} \quad \ldots \quad \text{(B-4)}$$

which is the expression for the one-step-ahead prediction of the current value of y given the input and past values of y. Because we do not know G^0 and H^0, we replace these terms with parameterized transfer functions, as represented in Eq. A-5. In addition, note that $G(q,\theta)$ and $H(q,\theta)$ are completely defined by n_a, n_b, n_c, and n_d. Finally, replacing the parameterized transfer functions into Eq. B-4 results in the so-called predictor model:

$$\hat{y}(k|k-1,\theta) = H^{-1}(q,\theta)G(q,\theta)u(k) + [1 - H^{-1}(q,\theta)]y(k). \quad \ldots \quad \text{(B-5)}$$

The prediction error for a model is

$$\varepsilon(k,\theta) = y(k) - \hat{y}(k|k-1,\theta) = H^{-1}(q,\theta)[y(k) - G(q,\theta)u(k)], \quad \ldots \quad \text{(B-6)}$$

where the last equality follows by substituting the expression for the predictor (Eq. B-5).

Appendix C—Spectral Analysis of Errors in Variables (EIVs) in Closed-Loop System Identification (SI)

The identification of R_{21}^d from just the bottomhole measurements is known as an EIV identification problem in a closed-loop configuration. To such a problem, neither a typical closed-loop SI method nor a typical EIV SI method is applicable. Söderström et al. (2013) have investigated the identifiability in such a configuration with the aid of a spectral analysis. In a spectral analysis, the auto-correlation signals of q_{bh}^m, p_{bh}^m, and their cross-correlation signals, on the basis of Eqs. 39 through 42, are calculated and then Fourier-transformed to form a set of algebraic equations:

$$\begin{aligned} \hat{\phi}_{p_{bh}}(\omega) &= |R_{21}W_{11}S|^2\phi_{q_{wh}}(\omega) + |S|^2\phi_{v_{p_{wh}}}(\omega) \\ &\quad + |R_{21}S|^2\phi_{v_{q_{wh}}}(\omega) + \phi_{\tilde{v}p_{bh}}(\omega), \end{aligned} \quad \ldots \quad \text{(C-1)}$$

$$\begin{aligned} \hat{\phi}_{p_{bh}q_{bh}}(\omega) &= R_{21}|W_{11}S|^2\phi_{q_{wh}}(\omega) + W_{12}^*|S|^2\phi_{v_{p_{wh}}}(\omega) \\ &\quad + R_{21}|S|^2\phi_{v_{q_{wh}}}(\omega), \end{aligned} \quad \ldots \quad \text{(C-2)}$$

$$\begin{aligned} \hat{\phi}_{q_{bh}}(\omega) &= |W_{11}S|^2\phi_{q_{wh}}(\omega) + |W_{12}S|^2\phi_{v_{p_{wh}}}(\omega) \\ &\quad + |S|^2\phi_{v_{q_{wh}}}(\omega) + \phi_{\tilde{v}q_{bh}}(\omega), \end{aligned} \quad \ldots \quad \text{(C-3)}$$

where the variables $\phi(\omega)$ and $\hat{\phi}(\omega)$ represent known and estimated spectral densities, respectively (as a function of frequency ω). R_{21}^d is then identifiable if the numbers of equations and unknowns at each frequency are identical. Note that the right-hand-side terms in Eqs. C-1 through C-3 can be estimated by use of the measurements, but that the left-hand-side terms are unknown, which illustrates that the noise terms make it impossible to obtain an estimate of $R_{21}(\omega)$.

One way to solve this identifiability issue is to make use of $q_{wh}(t)$. Because this auxiliary signal is uncorrelated with the bottomhole sensor noise and disturbances, the reservoir model may be estimated as

$$\hat{R}_{21} = \frac{\hat{\phi}_{p_{bh}q_{wh}}}{\hat{\phi}_{q_{bh}q_{wh}}}, \quad \ldots \quad \text{(C-4)}$$

where

$$\hat{\phi}_{p_{bh}q_{wh}} = R_{21}W_{11}S\hat{\phi}_{q_{wh}} \quad \ldots \quad \text{(C-5)}$$

and

$$\hat{\phi}_{q_{bh}q_{wh}} = W_{11}S\hat{\phi}_{q_{wh}}. \quad \ldots \quad \text{(C-6)}$$

This analysis concerns the formal identifiability requirements. To actually find the model, suitable closed-loop SI techniques should be used that can handle the noise and are more effective than spectral methods.

Appendix D—Modeling Gas Flow in an Infinite-Acting Reservoir

In a gas reservoir, the diffusivity and Darcy's equations are written as

$$\frac{1}{r}\frac{\partial}{\partial r}r\frac{\partial m(r,t)}{\partial r} = \frac{1}{\eta}\frac{\partial m(r,t)}{\partial t}, \quad \ldots \quad \text{(D-1)}$$

$$q_g(r,t) = -\frac{\pi rkhT_{SC}}{P_{SC}T}\frac{\partial m(r,t)(t)}{\partial r}, \quad \ldots \quad \text{(D-2)}$$

where T is the bottomhole temperature and where the pseudopressure is defined as $m(r,t) = 2\int_{p_0}^{p}\frac{p}{\mu z}\mathrm{d}p$ with p_0 as a reference pressure. The hydraulic diffusivity is $\eta = \frac{k}{\phi(\mu c_t)_i}$, where the viscosity/compressibility product is calculated at the initial reservoir pressure. T_{SC} and P_{SC} are temperature and pressure at standard conditions, respectively. For an infinite-acting reservoir, the boundary conditions are

$$q_g(r,t) = q_{sf}(t), \quad r = r_w, \quad \ldots \quad \text{(D-3)}$$

and

$$m(r,t) = 0, \quad r \to \infty. \quad \ldots \quad \text{(D-4)}$$

The partial-differential equation with boundary conditions is solved in a similar way as the partial-differential equation for the oil reservoir described in the body of the text, which leads to

$$\mathcal{M}_{sf}(s) = G_{\inf}(s)Q_{sf}(s), \quad \ldots\ldots\ldots\ldots\ldots\ldots \text{(D-5)}$$

where

$$G_{\inf}(s) = \frac{1}{\pi khr_w \frac{T_{SC}}{P_{SC}T}\sqrt{\frac{s}{\eta}}} \frac{K_0\left(r_w\sqrt{\frac{s}{\eta}}\right)}{K_1\left(r_w\sqrt{\frac{s}{\eta}}\right)}. \quad \ldots\ldots\ldots\ldots \text{(D-6)}$$

Adding the skin effect S_r to Eq. D-6 gives

$$G_{\inf,S_r} = G_{21} + \frac{S_r}{\pi kh \frac{T_{SC}}{P_{SC}T}}. \quad \ldots\ldots\ldots\ldots\ldots\ldots \text{(D-7)}$$

To simplify the notation, we use $G_{\inf}$ instead of G_{21,S_r}.

Appendix E—Conventional Deconvolution Applied to the Field Case

As a comparison with our proposed system-identification (SI) method, we applied a conventional deconvolution with the aid of commercial well-test-analysis software (Kappa Saphir 2015). To perform the deconvolution, it is necessary to approximate the flow-rate signal as a piecewise-constant signal. We tested two types of approximations: a fine approximation and a coarse approximation (**Fig. E-1**). The pressure signal is kept unchanged. To locate the constant-flow-rate periods, we used the wavelet-decomposition option in the software. An important and nontrivial step in the deconvolution method is the choice of the weights in the total-least-squares cost function:

$$\Phi = W_q R_q + W_p R_p + W_c C, \quad \ldots\ldots\ldots\ldots\ldots\ldots \text{(E-1)}$$

where W_q, W_p, and W_c are the flow rate, pressure, and curvature weights; R_q and R_p are residuals in the pressure and flow-rate estimates; and C is a measure of the curvature in the Bourdet derivative plot (von Schroeter et al. 2004). Because the accuracy of the pressure signal is higher, W_p is selected to be larger than W_q. The value of W_c determines the smoothness of the final solution and is of major importance in the optimization procedure. Several values of W_c have been tested with magnitudes between 0.01 and 5. **Figs. E-2 through E-4** depict the results for $W_c = 0.1$, 1, and 5, respectively. For smaller values of W_c, the deconvolved solution is strongly oscillatory, making it uninterpretable. We note that for this example, wellbore storage does not play a role, in line with the SI results, because the pressure and pressure-derivative plots do not display common values at early times (a characteristic feature for wellbore storage). For $W_c = 0.1$, the solution is still wavy, but interpretable.

Numerical type-curve matching, by use of an infinite-acting-reservoir model, gives the reservoir parameters as $k = 15$ md and $S = 0.1$ for the fine approximation and $k = 7.8$ md and $S = -2.9$ for the coarse approximation (Fig. E-2). For $W_c = 1$, k and S are 15.6

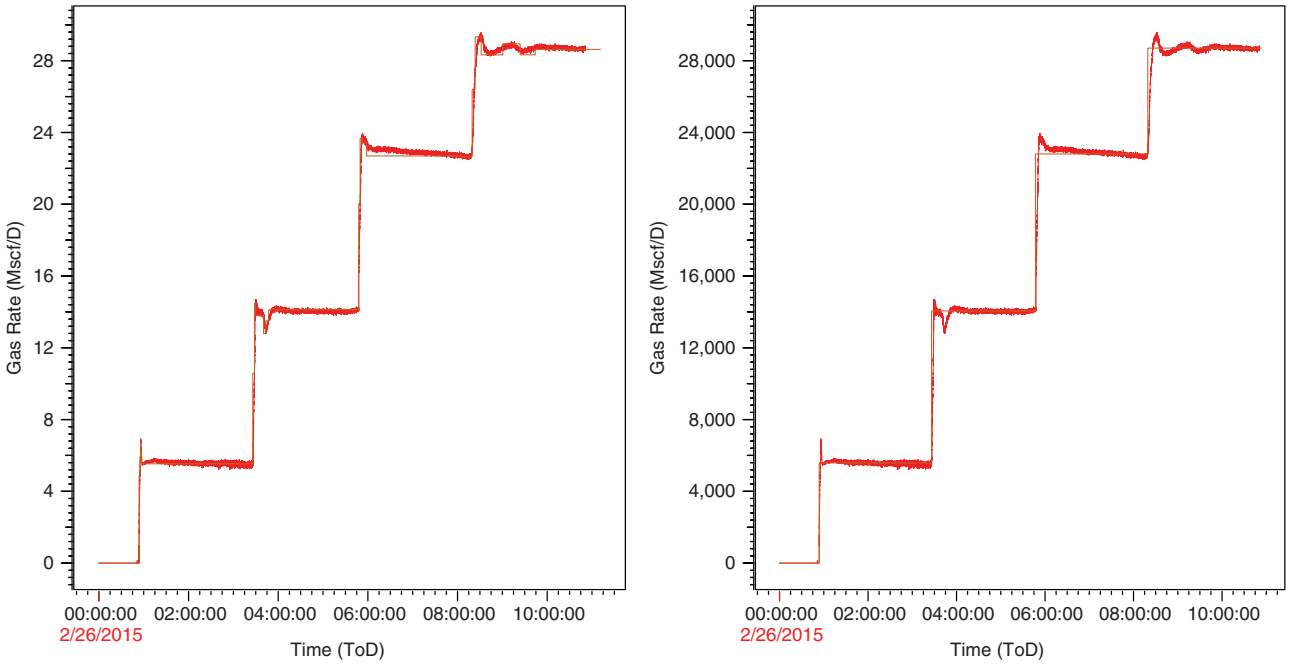

Fig. E-1—Fine (left) and coarse (right) approximation of the flow-rate signal.

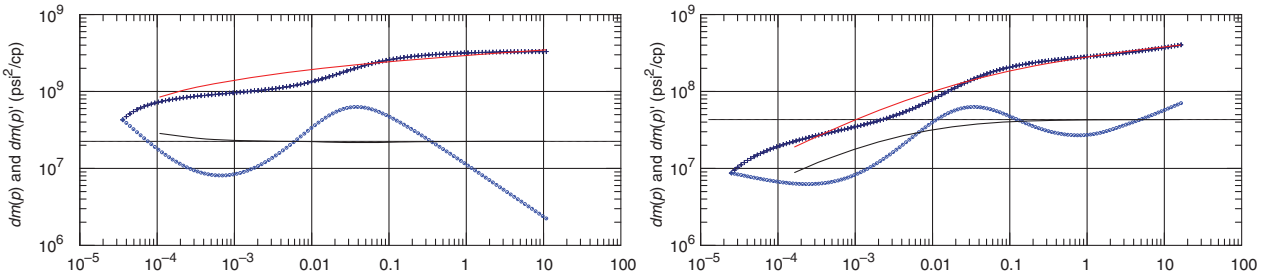

Fig. E-2—Deconvolution of fine (left) and coarse (right) approximations of the flow-rate signal for $W_c = 0.1$.

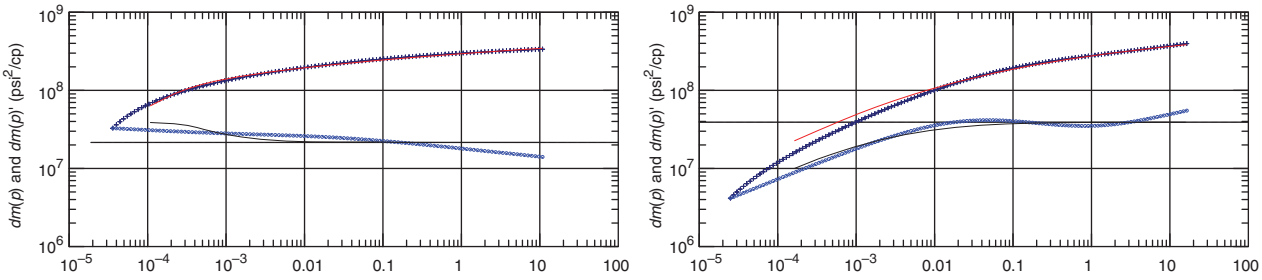

Fig. E-3—Deconvolution of fine (left) and coarse (right) approximations of the flow-rate signal for $W_c = 1$.

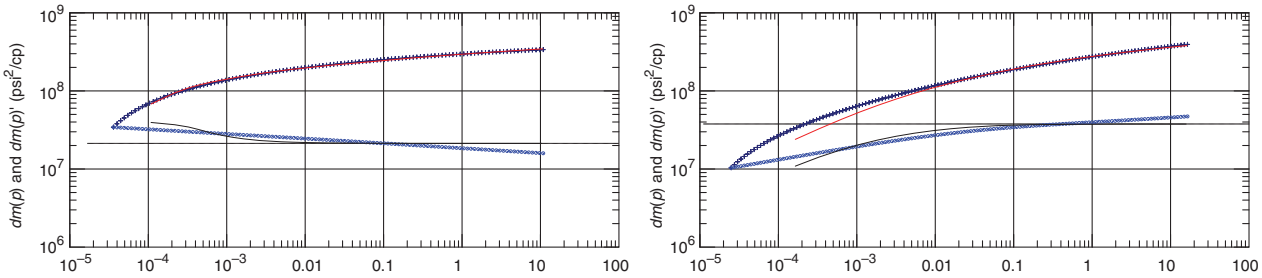

Fig. E-4—Deconvolution of fine (left) and coarse (right) approximations of the flow-rate signal for $W_c = 5$.

md and 0.4, and 8.6 md and −2.65 for the fine and coarse approximations, respectively (Fig. E-3). For $W_c = 5$, k and S are 15.8 md and 0.45, and 8.9 md and −2.53 for the fine and coarse approximations, respectively (Fig. E-4). Comparing these results with those obtained by SI and simple buildup analysis earlier in this study, the coarse-approximation results appear to be in the same range, whereas the fine-approximation results are significantly off. It is clear that the (somewhat-arbitrary) choice of the constant-rate approximation of the flow-rate signal can have a significant influence on the estimated parameters. In addition, the choice of the weight parameters influences the results.

Mehdi Mansoori is a PhD degree candidate in the Department of Chemical and Petroleum Engineering, Sharif University of Technology, Iran. Previously, he was a guest PhD degree candidate at Delft University of Technology, the Netherlands. Mansoori's research interests include pressure-transient analysis and system identification. He holds a master's degree in reservoir engineering and bachelor's degrees in mechanical engineering and reservoir engineering from Sharif University of Technology.

Paul Van den Hof is professor of control systems in the Department of Electrical Engineering at Eindhoven University of Technology, the Netherlands. His current research interests are in system identification and model-based control and optimization, with applications in several technology domains, including petroleum reservoir-engineering systems. Van den Hof holds master's and PhD degrees from Eindhoven University of Technology.

Jan-Dirk Jansen is professor of reservoir systems and control and head of the Department of Geoscience and Engineering at Delft University of Technology, the Netherlands. Previously, he worked for Shell International in research and operations. Jansen's current research interests are the use of systems and control theory for production optimization and reservoir management. He holds master's and PhD degrees from Delft University of Technology.

Davood Rashtchian is a professor of chemical engineering in the Department of Chemical and Petroleum Engineering, and currently the Dean of the Graduate School, of Sharif University of Technology, Iran. His research interests include safety and loss prevention in the chemical, petrochemical, and petroleum industries, along with reservoir engineering.